5-3-2023

Human Impacts on Erosion in Starved Rock State Park, Illinois, Usa

Savannah Leigh Thielbar
Illinois State University, slthie1@ilstu.edu

HUMAN IMPACTS ON EROSION IN STARVED ROCK STATE PARK, ILLINOIS, USA

SAVANNAH THIELBAR

60 Pages

State and National parks are some of the most visited wildlife areas within the United States, making local geologic features more susceptible to human-induced change. As more people visit these parks throughout the year, we see major impacts on the interactions between biological and geological processes. This study determines if human activity, through rock carvings, influence erosion within Starved Rock State Park and provides a new perspective on our compounding anthropogenic influence on Earth. Through natural stream and artificial human erosion, the base of the bedrock slope potentially changes at a much faster rate than the upper portion of the outcrop. By monitoring the fragile sandstone cliffs that preserve these human-created carvings, specific erosion data were collected in four different canyons within the park. Canyon wall data were collected and monitored using an Empire contour gauge, a Schmidt rebound hammer, and an iPhone 13 LiDAR camera with the 3D Scanner app program to determine seasonal variations in erosion throughout the park as well as the influence of surficial case hardening on the outcrops. The contour gauge and Schmidt hammer data collected suggest the bedrock of the area is affected on a small, millimeter scale within the course of a year. Data collected from the carvings compared to bedrock that is naturally eroding without human influence exhibits short-term localized changes to the bedrock that is greater than the long-term erosion of these surfaces. Analysis of Schmidt hammer values and thin sections indicate that some locations have stronger rock surfaces driven by differences in cement concentrations from the surface to the interior of the rock outcrops. Differences in rock strength produce variation in erosion across the canyons and provide context to seasonal processes that influence weathering. Future research

identifying the magnitude of this impact over a longer period, as well as potential difference between lithologies, can prove to be valuable in increasing education and awareness at other state or national parks.

KEYWORDS: Erosion, Rock strength, Anthropogenic influence, Starved Rock State Park, LiDAR, St. Peter Sandstone.

HUMAN IMPACTS ON EROSION IN STARVED ROCK STATE PARK, ILLINOIS, USA

SAVANNAH THIELBAR

A Thesis Submitted in Partial
Fulfillment of the Requirements
for the Degree of

MASTER OF SCIENCE

Department of Geography, Geology, and the Environment

ILLINOIS STATE UNIVERSITY

2023

HUMAN IMPACTS ON EROSION IN STARVED ROCK STATE PARK, ILLINOIS, USA

SAVANNAH THIELBAR

COMMITTEE MEMBERS:

Lisa Tranel, Chair

Eric Peterson

Wondy Seyoum

Dave Malone

ACKNOWLEDGMENTS

First, I would like to thank my thesis advisor, Lisa Tranel, for allowing me to take this research in the direction that peaks my interests and passion. Without her mentorship and guidance, my time at Illinois State University would not have been this fun and successful. Lisa and the other facility members at ISU, especially my thesis committee, are always available to offer me suggestions or just check in with me. I'd like to also thank the Office of Student Research for awarding me with funds through the BirdFEEDER Grant to collect and analysis my data from the field.

Secondly, I am forever grateful to my fellow graduate classmates. They've always been an outlet to go to when needing some reassurance or just a friendly pick-me-up. Being able to share the struggle and thrive in the success together strengthened my drive to be my best every day.

Thirdly, a fellow undergraduate student who was instrumental in this study by collecting and analyzing thin section data was Addie Bowen. Her work in Starved Rock helped drive comparisons with other data collected while adding useful information and resources to this study.

Lastly, my family and friends are always my number one supporter in anything I do. Without their constant positivity, I would not be where I am today. Believing in my passion and abilities enabled me to develop into the amazing person and geologist I continue to be every day and I will forever be grateful.

ST

CONTENTS

TABLES

FIGURES

CHAPTER I: INTRODUCTION

State and national parks are some of the most visited wildlife areas within the United States, allowing the local geology to become more susceptible to human-induced change. As more people visit these parks throughout the year, we see major impacts on wildlife, plant life, and the geological structures present (Ancin-Murguzur et al., 2020). Multiple concerns arise from these impacts and this study begins to identify the magnitude of human influence on the canyon walls within the park.

Illinois's Starved Rock State Park has seen record numbers of visitors recently, with more than 2.8 million people visiting in 2017 (Montecillo, 2018). That number surpasses all but 10 of the country's 58 national parks, and Starved Rock has become so popular that maintaining it has become extremely challenging. Since this park is frequently visited throughout the year, we see evidence of human activity along the trails and on off-path outcrops. In addition to the natural processes of bedrock undercutting by the various waterfalls throughout the park, groundwater sapping and seasonal changes in climate, as well as anthropogenic processes affect the brittle geology of the park (Irvine, 2001). By estimating the magnitude of human influence on erosion within the park, we identify if those impacts will have long-term consequences for this State Park.

Within Starved Rock there are areas where visitors venture off-trail, which is proven by carvings occurring along the trails and in out-of-the-way locations where the canyon walls are accessed with ease. Past work in Starved Rock by Rutte et al. (2018), initiated an investigation on the impacts of humans throughout the park. Her work analyzed the short-term erosion potential of the St. Peter Sandstone within the park to identify how erosion has changed from the last glaciation

event to today. Other researchers have also done studies on archeological sites, to better understand the erosional processes of "cultural stone", created by human activity, and how those affects altered the natural state of the rock surfaces (Pope et al., 2002; Dorn et al., 2008; Kamh & Koltuk, 2016). ''Cultural stone'' is a term used for rock that has been physically altered by humans. It includes architectural stone, rock art and other rock engravings, and carved stone ornaments (Pope et al., 2002; Dorn et al., 2008). All involve anthropogenic removal of rock to expose a new surface.

This study attempts to understand the internal and external factors affecting natural erosion of human-induced disturbances along the bedrock wall by targeting study sites that are easy to access and provide high frequencies of carvings (Figure 1). Internal controls include the petrology of the St. Peter Sandstone because porosity, grain size, mineral composition, and cement concentration can influence cohesion between bedrock grains and rock strength (Chang et. al, 2006). External forces related to climate, vegetation cover, water influence, or land use and direct interaction control natural weathering within this area. To identify differences among the bedrock outcrops, we combined contour gauge weathering profiles, petrographic thin sections, and Schmidt hammer rock strength data to measure the total change of the carved surfaces compared to the undisturbed bedrock. Variations in rock strength of the undisturbed bedrock across the park allow for further investigation of the formation and breakdown of case hardening and the role of vegetation for protection or deterioration purposes. We expected our results to show carved surfaces experiencing higher rates of change than unaltered surfaces.

The study also included 3D LiDAR scans of each canyon wall to identify regions on the surface where more erosion is prominent. Comparing scans taken months apart provided an analysis of the magnitude of erosion occurring within the timeframe over the entire bedrock wall

face. Limitations to this method were identified when comparing scan results, prompting an evaluation of techniques and conditions that are best suited to collecting field data.

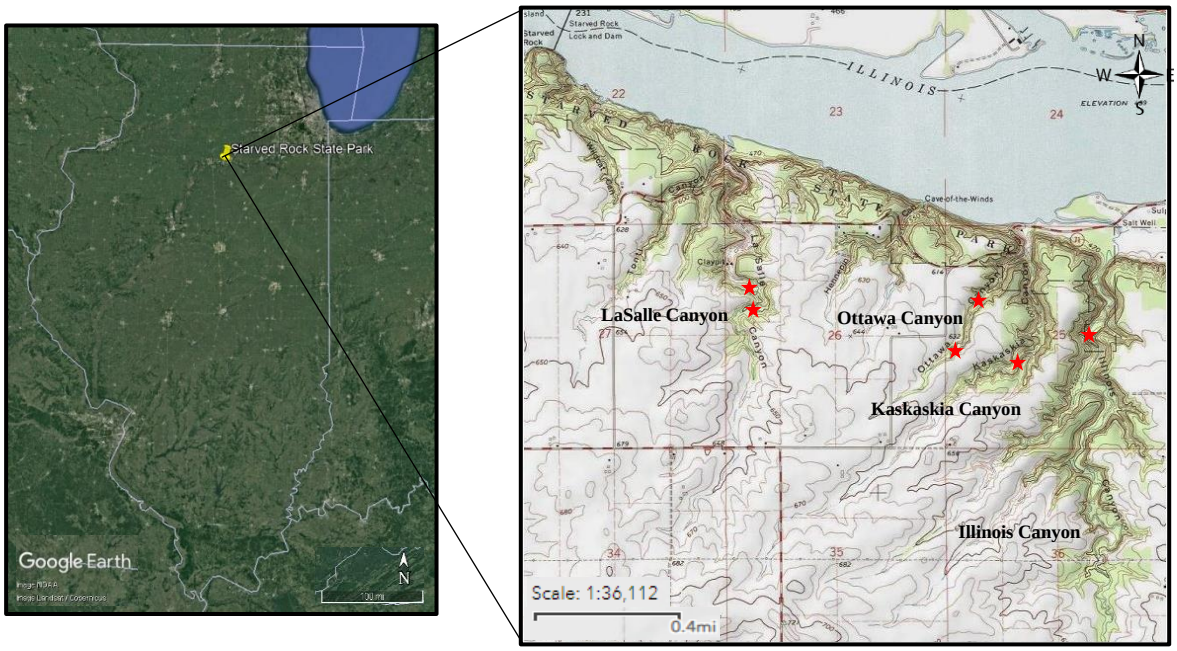

Figure 1: Reference map of Starved Rock State Park, IL provided from Google Earth. Left image shows geographical location of the park. Right image is a topographical representation of the eastern area of the park where methods were executed. Stars represent targeted canyon data collection locations (LaSalle, Ottawa, Kaskaskia, and Illinois Canyon). Image edited from Topozone.com.(https://www.topozone.com/map-print/?lat=41.3130899&lon=88.96758&title=Starved Rock State Park Topo Map in LaSalle County Illinois)

Research Questions

We aim to understand the processes of natural erosion that is influenced via human interactions by comparing undisturbed and human-altered bedrock surfaces on canyon walls within the park. We hypothesize that human carving will affect the bedrock's natural processes of erosion during our 1-year study. We focus on the following research questions:

1. Does carving into the bedrock accelerate the erosion of that surface?
2. Does a high variability in rock strength influence erosion across the park?
3. Does the age of the carvings influence erosion over time?
4. How are seasonal variations affecting erosion in each of the canyons?
5. Are millimeter scale changes to rock surfaces detectable with iPhone LiDAR technology?

CHAPTER II: BACKGROUND

Illinois' surficial geology is mainly defined by past glacial advancements and retreats including the Pre-Illinois, the Illinois, and the Wisconsin Glaciations (Nelson, 1996). From the most recent Wisconsin glaciation event, the topography of north-central Illinois resulted in low-relief rolling hills, thick glacial deposits, and unique bedrock canyons (Huysken et al., 2016). In Starved Rock we see exposed rocks that protrude from the bluffs within the park and along the Illinois River. Following the most recent ice age, the Illinois River formed as glacial meltwaters flowed through the Illinois River valley and began to erode the landscape. The Kankakee Torrent event then caused meltwater from nearby melting glaciers to funnel water through the Illinois River, widening, and deepening the valley, reducing its base level (Willems et al., 2007; Curry et al., 2014). The Illinois River and its tributaries are now remnants of historical glacial streams produced from meltwater floods that over time incised into the Ordovician St. Peter Sandstone creating the massive sandstone cliffs we see in the park today (Curry et al., 2014; Huysken et al., 2016).

Within the park the exposed bedrock is composed of mostly one Ordovician sandstone unit, the St. Peter Sandstone, which is a weakly cemented, friable quartz arenite (Huysken et al., 2016). There are two members of the St. Peter Sandstone, the Starved Rock, and the Tonti Member. The Starved Rock Member is the uppermost member of the St. Peter Sandstone and is commonly 60-100 feet thick and occurs in a broad band, extending southwestward from the Chicago area to the Mississippi River in the Quincy area (Davis, 2014). The Starved Rock Member differs from the Tonti Member in being mostly composed of medium grains rather than fine grains and preserving more cross bedding (Nelson et al., 1996). At Starved Rock, the lower part of the member contains

thin beds that are poorly sorted. The St. Peter Sandstone found within Starved Rock is composed of nearly 100% well, rounded quartz grains, with a bimodal size distribution of 0.1–0.2 mm and 0.35–0.45 mm (Haimson & Klaetsch, 2007). Quartz overgrowths, with little or no iron oxide cement, bind the sandstone framework structure together. The porosity of the St. Peter Sandstone varies but can be summarized as being either 11 –12% ('low porosity') or 16– 22% ('high porosity') (Hoholick et al., 1984; Haimson & Klaetsch, 2007). Because it is very weakly cemented, we expect to easily detect and monitor changes along the bedrock.

Biogeochemical processes that help mitigate erosion, like case hardening, rock varnish and lichen or moss cover, are present throughout the park and provide some natural method of preservation. Over time, rocks exposed at the surface develop weathering rinds through case hardening, which "is the process by which the outer shell of an exposed rock surface hardens due to near-surface diagenesis" (Dorn et al., 2017). Weathering rinds are derived from mineral dissolution, precipitation of dissolved constituents, and mechanical fracturing of the outer millimeters of a rock to create porosity (Dorn et al., 2017). Ongoing reactions with rain, frost, or groundwater result in the downward migration of rock-coating components into weathering rind pores (Pope et al., 2002). Initially, if those exposed pores are filled, it will protect the outer surface of the rock from flaking or exfoliating, increasing resistance to erosion. As case hardening progresses, however, ongoing mineral dissolution underneath the weathering rind could eventually lead to detachment and increases in erosion (Dorn et al., 2008). First this process helps strengthen the structural integrity of the bedrock walls, until the protective shell is removed or disturbed, exposing new, weakly cemented grains to increased erosion.

Other biogeochemical reactions influencing erosion within the park include the presence of lithobionts, biofilms, and other microorganisms. The growth of lithobionts on stone surfaces has long been associated with biodeterioration (Favero-Longo et al., 2020). Biogeochemical effects of organisms might promote salt and frost wedging by increasing pore volume and moisture content, precipitation of sulphates and oxalates, and mineral alteration or they may inhibit the effectiveness of salt weathering by reducing effective porosity and permeability, preventing pollutant accumulation, and altering thermal characteristics (Turkington & Paradise, 2005). These controls on erosion processes, such as moisture availability, may be perceived as enhancing rates of all types of processes: whereas other types of controls, such as atmospheric pollutant concentrations, may increase processes like salt wedging (Gordon & Dorn, 2005). Across a range of spatial scales bryophytes, lichens and microorganisms anchor or adhere to mineral substrates to provide stability, exploit water and/or nutrients, and consequently they can modify the physico-chemical properties of the substrates. In doing so, initial removal of these lithobionts can result in an increase in erosion of the surface. In some cases, they offer an umbrella-like protection from pollutants across bedrock walls (Favero-Longo et al., 2020). Biodeterioration is a much slower process than physical and chemical weathering of sandstones in this environment, and therefore lichen represent a protective cover for the bedrock over certain timescales (Carter & Viles, 2005). Additionally, experimental studies illustrate that certain types of lichen can protect vulnerable bedrock walls from freeze–thaw damage through modifying microclimatic conditions (Coombes et al., 2018). In drier climates, rock surface microorganisms are chemically involved in the development of rock coatings, which stabilize the rock surfaces and contribute to their long-term preservation (Favero-Longo et al., 2020).

CHAPTER III: METHODOLOGY

Contour Gauge Analysis

Contour gauge analysis was executed on targeted carvings within Starved Rock State Park. The Empire contour gauge serves as a user-friendly and cost-effective tool to investigate mm scale changes along a surface (Adams et al., 2014). A contour gauge is a tool, 15 cm wide with 181 independently moving 0.8 mm diameter pins, used to measure surface roughness (Shobe et al., 2017). Our maximum extent of precision with this tool was 0.8 mm, with a pin depth range of 45 mm. To maintain accuracy the rods were lined up to form a baseline, the gauge was then pressed against the surface at designated vertices, allowing the pins to move independently, recreating the surface profile (Adams et al., 2014). In the field, contour profiles or "weathering profiles" of each carving were recorded in a field book and then transferred onto 1 mm graph paper to represent a simple linear profile. Gauge endpoints were marked with a permanent marker (Sharpie), to avoid any disturbances on the surface and to ensure consistent data analysis and comparison when collecting repeated measurements in the field (McCarroll & Nesje, 2008). Each site included additional measurements on a control profile to compare erosion rates between carvings and undisturbed bedrock. Control locations were based on location relative to the carving(s) and degree of roughness. Surfaces with no recent natural or human interactions present next to the carvings were used to compare with the rate of erosion associated with carvings.

Observations were repeated every two months to quantify overall differences in surface roughness and show discrepancies related to seasonal variation. Profiles were digitized from 1 mm graph paper using PlotDigitizer, a free online based software and app that allows users to extract numerical data from several types of plots, graphs or images to create a table of XY coordinates

or values (Drevon et al., 2017). To extract XY coordinates, this software requires users to import graphs, calibrate axes by clicking known values for the tool to interpolate a coordinate system, and manually click each data point in a data series. Exporting the coordinates in a comma separated values (.csv) file to Excel allows for graphical and numerical analyses and comparisons. Previous research done by Aydin & Yassikaya (2022) show that extracting digitized values from graphs with the PlotDigitizer on different operating systems offers valid and reliable results at high coefficients, meaning decimal values must be converted to the nearest integer to be used in further analysis.

Profile vertices were aligned using the X-intercept as the datum for consistency and plotted in 5 mm increments across the profile. Establishing a datum line that represents the Sharpie marks on the surface when digitizing a profile allows for simple standard deviation and difference analysis calculations. Using the datum line and plotting in 5 mm increments produced the same X-values for each repeat profile to capture the changing Y-values representing erosion on the rock surfaces. The mean and standard deviations of the differences between the Y-values were analyzed for each carving and associated control in Excel to determine the effects of carving on the bedrock.

Rock Strength Analysis

Carving study locations correspond to access and distance from the trail and occur in areas close to the active stream channels. Study sites in LaSalle, Ottawa, and Kaskaskia Canyons include carvings located near areas where surface water influence is present. In Illinois Canyon, access across the active stream channel was limited based on water level, causing some potential sites to be unreachable for most of the year. Therefore, one carving location within this canyon lies farther from the stream channel than the other carvings and an additional site was added to the study to

account for that location of the canyon influenced by the stream. Constant water action can initiate case hardening processes from the mineralization of pores, but also can cause undercutting of the bedrock through mechanical weathering. The strength of rock found within the canyons was used to describe any discrepancies found with the contour gauge and LiDAR results.

Strength measurements were performed on six bedrock outcrops associated with targeted carvings during the month of July. Measurements were executed on one additional bedrock site located near the stream bed in Illinois Canyon to account for any discrepancies in rock strength provided by the stream influence. The position of the carving relative to the stream bed may contribute to the erosivity of the bedrock due to the water influence on bedrock strength as well as access for human interaction and carving. Strength measurements were collected and recorded in megapascals (MPa) with an N-type Schmidt hammer to test for correlations between different factors influencing erosion, including porosity or cement and the strength of the rock. A Schmidt hammer test is a non-destructive testing method which provides a convenient and rapid indication of the rock's compressive strength (Aydin & Basu, 2005). The Schmidt hammer operates with a spring-controlled mass that slides on a plunger within a tubular housing. When the plunger of the hammer is pressed against the test surface, a spring-controlled mass with a constant energy hits the surface and bounces back, giving a rebound value (Shobe et al., 2017).

Schmidt hammer strength profiles were created from the base of the outcrop to the area of the carving to test for physical differences across the sandstone and impacts of carvings on rock strength. Using a tape measure, chalk and a Schmidt hammer the canyon wall was divided into 1 m x 0.5 m sections starting from the stream bed, canyon floor or trail, depending on location, to the top of the carving. Across each section, 25 single hits were executed to produce an average

strength for each section. A minimum of 10-30 hits on a single section of bedrock is recommended when producing Schmidt hammer data sets (Shobe et al., 2017). Conducting 25 single-hits provided information about the heterogeneity of bedrock, showing variation within the data, and controlling error from micro-compaction resulting from repeated hits (Aydin & Basu, 2005). Average strength values were used to create a strength profile and identify deviation within the section of the bedrock to supply connections between physical, chemical, and biological influences to allow for accurate comparisons of erosion between the different canyons (Cerna & Engel et al., 2011; Shobe et al., 2017).

Petrographic Analysis

Hand samples were collected in each of the targeted canyons from the surface of relatively fresh rock falls to identify the influence of case hardening on natural erosion. Of the four rock samples, two were collected in 2020 by a previous researcher (LTLS20-01 and LTIL20-04), while the other two were collected in 2022 (STOC22-02 and STKC22-03). The fragile samples were sent to Wagner Petrographic in Lindon, Utah to undergo epoxy impregnation to fill in any pore spaces and strengthen the integrity of the rock for cutting purposes. Blue epoxy was chosen to allow for an easy visualization of grains and cement under magnification. Once returned, grain area, pore space, and amount of cement are digitized using a computer program, NIS Elements Viewer, developed by Nikon, to estimate whether the percentage of cement and its removal affect bedrock erosivity. Eight times magnification was used for digitizing grains, pore spaces, and cement from regions at the top (outside surface) of each thin section slide. Digitizing was completed by an undergraduate research student and uploaded into a shared Excel document for basic percentage calculations.

Thin section areas are totaled to determine percentage of grains, pore space, and cement within rock falls located in each of the four study sites. Results were compared to determine if spatial variation in percent cement was seen across the study region and the influence of its removal on natural erosion. Focusing on the outermost 5 mm of the sample will determine if carving removes the bedrock's surficial protective coating and consequently increases the vulnerability of the bedrock to erosion.

LiDAR Analysis

In 2020, Apple© implemented a Light Detection and Ranging (LiDAR) sensor in the new Apple iPad Pro (4th Gen) and iPhone Pro 12. Since then, LiDAR collection is available in these new Apple devices and allows access to LiDAR-generated 3D point clouds on consumer-level devices (Gollab et al., 2021). Apple's newly patented LiDAR system, TrueDepth©, uses vertical-cavity surface-emitting laser (VCSEL) technology and consists of a traditional camera, an infrared camera, a proximity sensor, and a dot projector (Łabędź et al., 2022). The dot projector emits more than 30,000 points of infrared light, which are reflected from surfaces. The infrared camera picks up these light dots and the pattern is analyzed by the phone application to create a depth map. Using this depth map, a mathematical model is generated by machine learning algorithms (Vogt et al., 2021).

Apple itself does not specify the accuracy of the respective technologies but, from the literature available, it can be deduced that the sensor range is about 5 m (Łabędź et al., 2022; Gollab et al., 2021; Luetzenburg et al., 2021). While the hardware and the software of the device determine the scan accuracy internally, external factors like reflectance, shape and color of the object as well as surface texture and ambient lighting influence scan quality. In addition, the

distance between object and scanner, scanning strategy and scanning movements can influence scan quality but the iPhone's orientation and angle do not need to be regarded during scanning (Vogt et al., 2021; Luetzenburg et al., 2021). The new Apple © LiDAR devices' primary field of application is small to medium scale rapid changing morphological features, ranging in size from centimeters up to several hundreds of meters. This tool can be used in many different disciplines including bio- and geosciences, however, since this technology is so new, very few publications exist on the performance of this new sensor and on its possible application areas (Vogt et al., 2021).

The LiDAR tool was used at four carving study outcrops. The walking speed, height of the iPhone 13 Pro Max (2022) (1.2 m), distance from the outcrop, and scanning strategy were kept constant while collecting data. Size of the scan, distance from the outcrop and lighting conditions were variable across all scans (Table 1).

Table 1: Scan technique and outcrop dimensions for original alignment scan (November of 2022) used for further segmentation.

Original Scan Dimensions and Conditions						
Canyon	**Carving Name**	**Distance from rock surface (m)**	**Outcrop Length (m)**	**Width (m)**	**Height (m)**	**Lighting Conditions**
LaSalle	*Vazquez*	2.5	1.6	2.9	2.5	Shaded by Overhang
Ottawa	*Tony + Jean*	1.0	0.9	2.0	1.7	Shadows from Trees
Kaskaskia	*Trent*	1.5	1.0	2.0	1.5	Shaded by Overhang
Illinois	*PXV*	2.0	1.0	5.8	2.2	Shadows from Trees

For this study, scans were produced from the 3D Scanner App (Laans Labs) using an Apple© iPhone 13 Pro Max and transferred into CloudCompare for analysis. With this application, 3D models are generated from the LiDAR data and can be processed into low resolution (>1.5 cm) and high resolution (<1 cm) data sets (Costantino et al., 2022). The "low res" has no parameters

to set and provides the simplest mode to capture a 3D scene, which is recommended for larger than 5 m scans. The “high res” allows the operator to produce a better scan, offering four different settings: “max range” (ranging between 1 m and 5 m with a step of 0.1 m), “simplify” (ranging from 0% to 90%), “smoothing” (ranging from 0x to 4x) and “voxel size” (ranging from 3mm to 21mm) (Teppati Losè et al., 2022). The accuracy of the 3D Scanner software relies on scan size and technique and has an accuracy of ~2 mm dependent on scan conditions (Laan, 2022). Processed scans were exported in the highest resolution: voxel size of 3 mm, smoothing “off”, simplify “off”, and max range of 5 m. Scans were taken twice during the study period, once in November 2022 and once in January 2023. Because our methodology evolved during the research, scans were not done at the beginning of the study period, but still allow for visual, qualitative comparisons between the canyons and provide additional knowledge on the effects of seasonal variation on erosion.

Scans were exported from the 3D Scanner App software as a high-density Point Cloud formatted .LAS file and imported into CloudCompare software on a computer. This format works well with the tools and features provided within CloudCompare to manipulate and to analyze the data. Both the November and January point clouds were imported to CloudCompare, and the point sizes were increased to six to allow for an accurate alignment. A new set of overlayed scans was produced by highlighting both sets and using the “Align two Point Clouds” tool from the dropdown menu. Four points needed to be picked to process the alignment using the older (November 2022) scan as the reference and the newer (January 2023) scan as the aligned. Once aligned, the reference scan was split into x,y,z components using the “computing cloud-to-cloud distance” tool. The Cloud-to-Cloud method (C2C) computes distances between two point clouds or between a point

cloud and a mesh. The basic C2C distance computation method calculated the nearest neighbor distance between the reference cloud and the compared cloud datasets. The principle of nearest neighbor distance was used to compute the distances between the two points where the nearest point in the reference cloud was searched and the Euclidean distance was computed for each point in the compared cloud (Ahmad Fuad et al., 2018). By using the November scan as the reference, the model shows the change on the surface as distance from November to January. Once the computation was complete, the color scale was adjusted in the "Properties" of the compared entity to display the results clearly. The segment tool was also used to crop out areas along the margins of the data where the scans were not directly overlayed and outside of the area containing features of interest for this study. LiDAR scan segmentation was used to reduce noise and define the area of interest. Segmentation dimensions are listed in Table 2. Other tools within CloudCompare provided calculations for RMS error, ranges, and histogram data that were exported and used for result analysis.

Table 2: Scan segmentation dimensions for each canyon scan to observe changes on the targeted surface where carvings reside.

LiDAR Scan Segmentation				
Canyon Location	**Carving Name**	**Length (m)**	**Width (m)**	**Height (m)**
LaSalle Canyon	Vazquez	0.29	1.0	0.71
Ottawa Canyon	Tony + Jean	0.36	0.72	0.59
Kaskaskia Canyon	Trent	0.13	0.96	0.65
Illinois Canyon	PXV	0.13	0.65	0.67

CHAPTER IV: RESULTS

Contour Gage Analysis

Contour gauge analysis produced a large variation throughout our sample set. Contour profiles were plotted overlapping (See Appendix), with only y-values changing, allowing for roughness and variation calculations in Excel. Once plotted, a mean profile was calculated from the sum of the y-values per x-value and graphed showing the standard deviation (See Appendix). A box-whisker plot was created showing combined y-value data from all field visits for each carving and control site. These data were used to compare the roughness of the carved surface to our controlled surface (Figure 2).

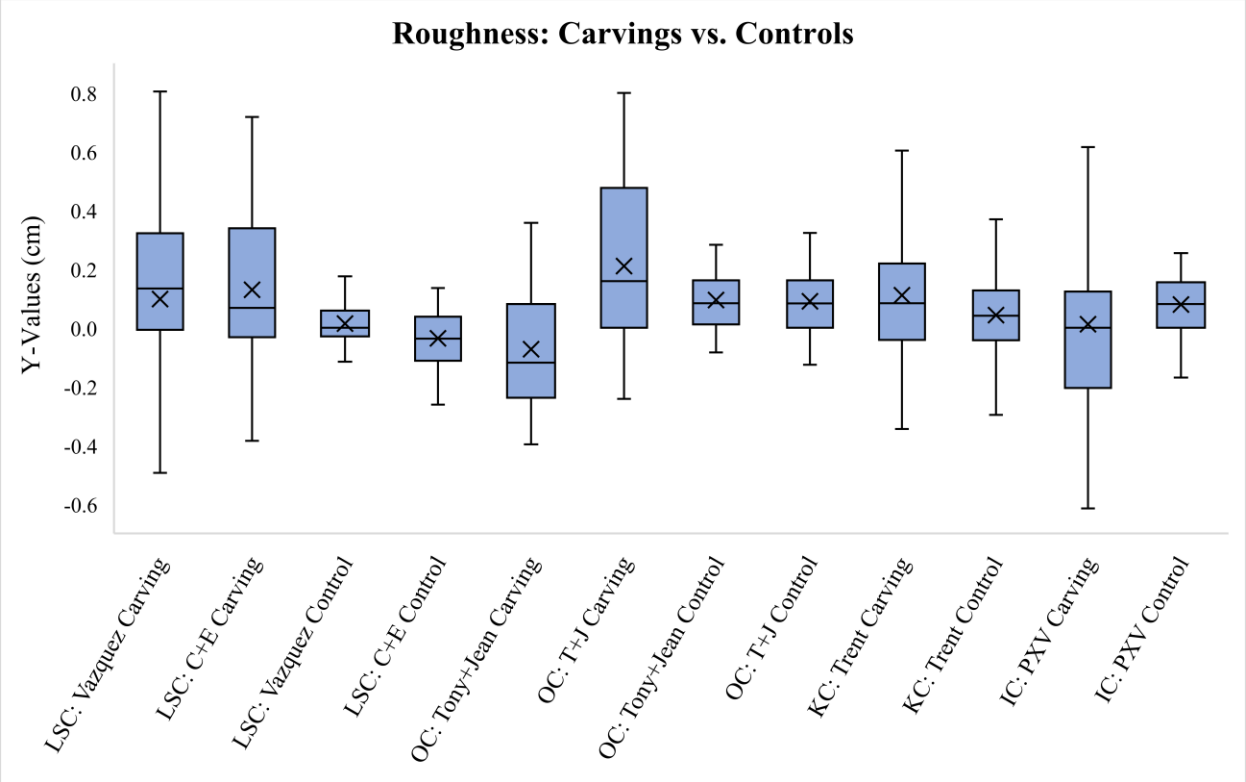

Figure 2: Box-Whisker Plot of cumulative carving data within each canyon and associated control data. Y-values from contour profiles show overall roughness of targeted surfaces. Error bars, outliers and mean values were calculated by Excel. Positive values are associated with the carved bedrock (into the bedrock), and negative values can be attributed to areas between the carved letters or bedrock protruding from the surface (out of the bedrock), and values located at 0.0, lie on the datum (flat).

The carved surfaces within the canyons exhibit a larger surface roughness than the control surfaces. These differences are seen within both the Box-Whisker plot (Figure 2) and contour weathering profiles (See Appendix).

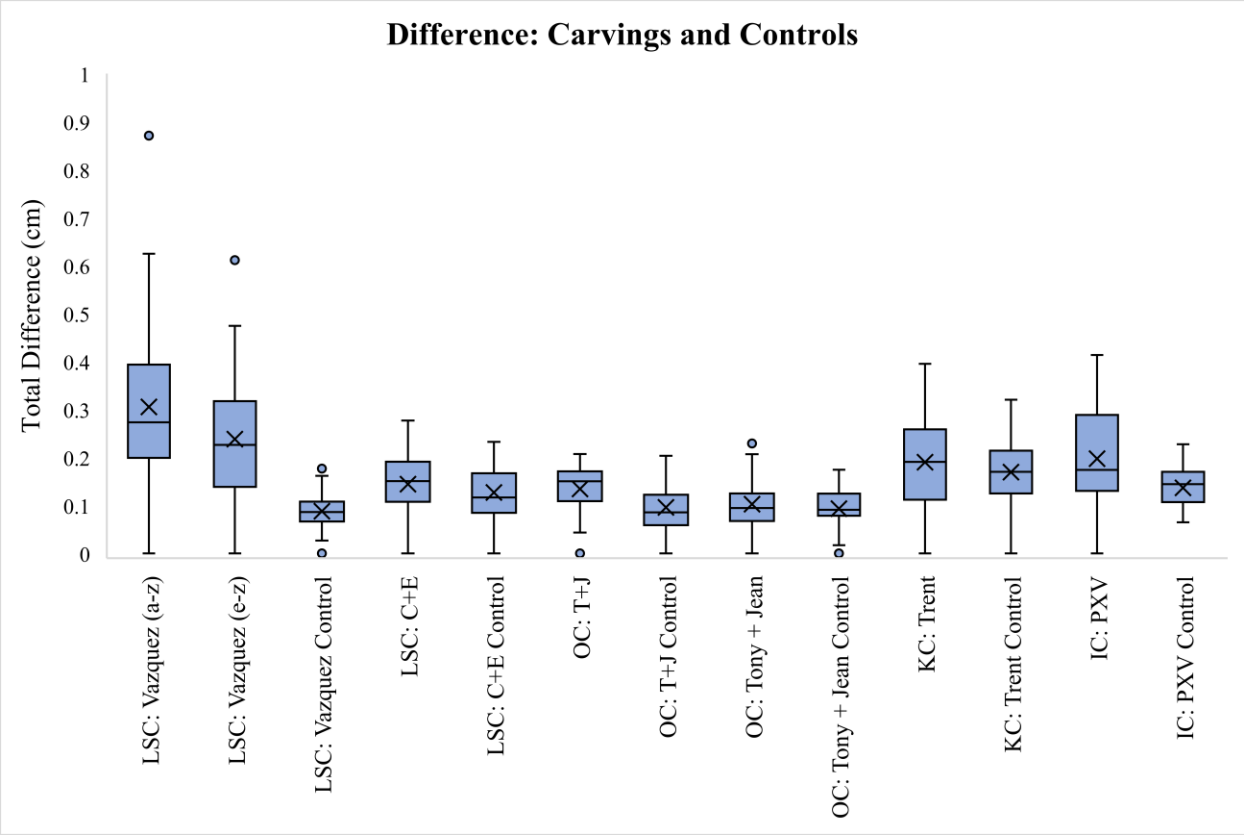

Figure 3: Box-Whisker Plot of cumulative carving data and associated control data. Difference from maximum and minimum values from contour profiles show average change between targeted carvings and undisturbed bedrock represented by the control observations. Error bars, outliers and mean values were calculated in Excel. Locations marked with an X signify the average change and are listed and described below in Table 3.

The difference values calculated from the maximum minus the minimum of all timeseries data were plotted to identify the maximum possible change of the carved surfaces versus the targeted controls (Figure 3). Average change values from Figure 3 show the difference in erosion between the canyons and their respective control profiles (Table 3). LaSalle Canyon's "*Vazquez*

(a-z)" (3.1 ± 1.8 mm*)* and *"Vazquez (e-z)"* (2.4 ± 1.3 mm) profiles had the greatest change of the carvings, whereas Ottawa Canyon's "*Tony + Jean"* carving had the lowest change of 1.0 ± 0.5 mm. All the control profiles resulted in similar differences, landing between a range of 0.9 ± 0.4 mm to 1.4 ± 0.6 mm, except Kaskaskia Canyon's "*Trent"* control which resulted in a 1.7 ± 0.7 mm change.

Table 3: Results from contour gauge difference calculations. Average change values are the same as the mean (X) located on the Box-Whisker Plot in Figure 3. Conversions from centimeters to millimeters allowed for units to remain constant throughout the analysis.

Contour Gauge Results		
Canyon Location	**Carving Name**	**Average Change (mm)**
LaSalle Canyon	Vazquez (a-z)	3.1 ± 1.8
LaSalle Canyon	Vazquez (e-z)	2.4 ± 1.3
LaSalle Canyon	Control	0.9 ± 0.4
LaSalle Canyon	C+E	1.4 ± 0.6
LaSalle Canyon	Control	1.2 ± 0.6
Ottawa Canyon	T+J	1.3 ± 0.6
Ottawa Canyon	Control	0.9 ± 0.5
Ottawa Canyon	Tony + Jean	1.0 ± 0.5
Ottawa Canyon	Control	0.9 ± 0.4
Kaskaskia Canyon	Trent	1.9 ± 1.0
Kaskaskia Canyon	Control	1.7 ± 0.7
Illinois Canyon	PXV	2.0 ± 1.0
Illinois Canyon	Control	1.4 ± 0.6

Results from the LaSalle and Illinois Canyon contour gauge profiles confirm erosion is more prominent along areas of freshly exposed bedrock than areas that are undisturbed. Ottawa and Kaskaskia Canyon's carving and control profiles resulted in smaller variations between the surfaces. Measurements from the Schmidt hammer will also be discussed below to provide insight into differences seen amongst the canyons.

Seasonal variation was visualized by comparing the total change between the carvings and controls during the cold months (January 22', March, and January 23') and warm months (May, July, and September) (Figure 4). From the Box-Whisker plot, the most recent carvings, LaSalle Canyon's "*Vazquez"* and Ottawa Canyon's "*T+J"* carvings and controls both show higher amounts of change during the cold months versus the warmer months. Kaskaskia and Illinois Canyon's carving and control, however, resulted in more change occurring during the warm months while Ottawa Canyon's *"Tony + Jean"* carving and control show minimal differences.

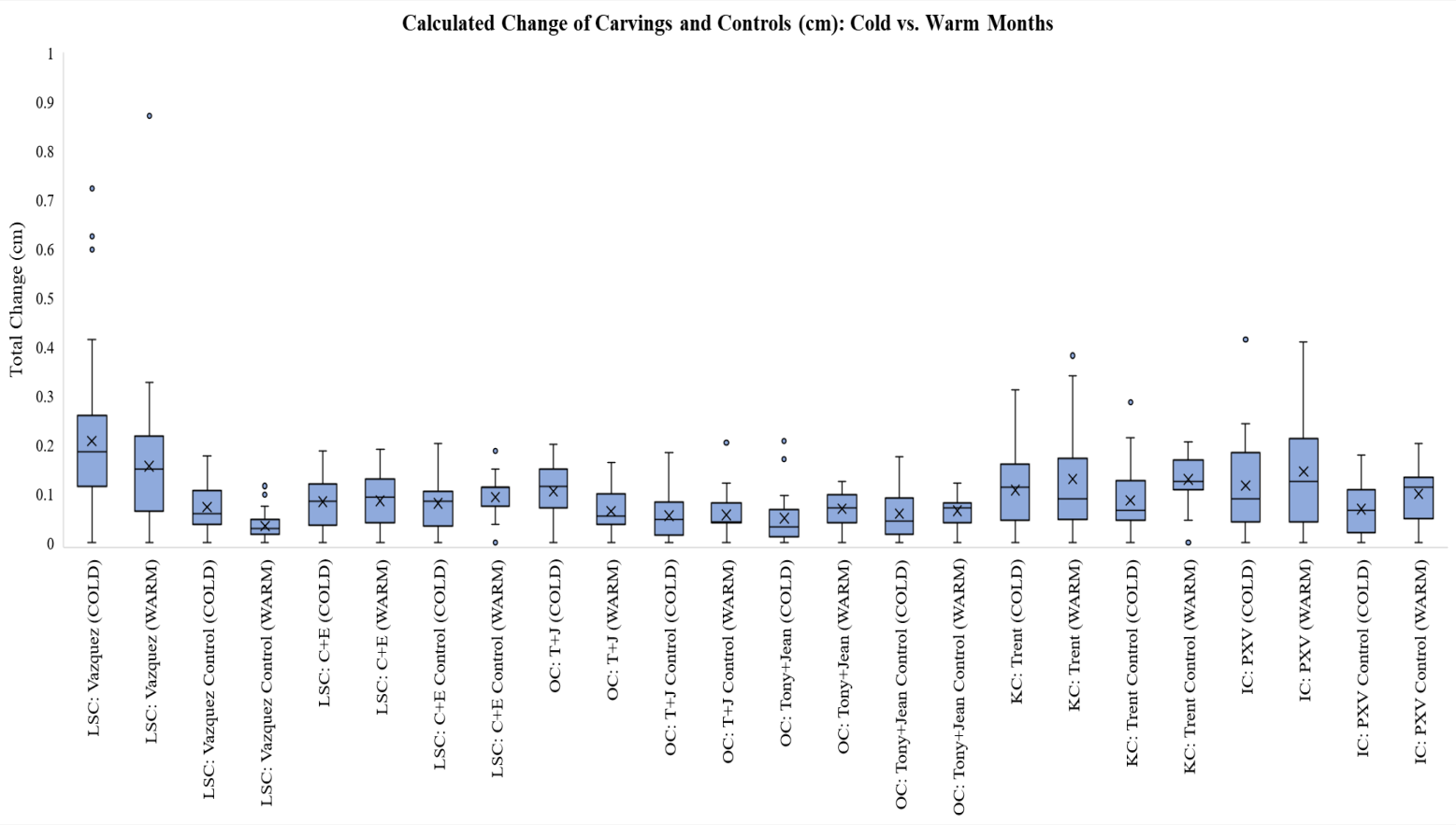

Figure 4: Box-Whisker Plot of cumulative carving data and associated control data. Change values calculated from contour profiles show seasonal variations between targeted carvings and undisturbed bedrock during cold and warm months. Error bars, outliers and mean values were calculated in Excel.

Rock Strength Analysis

Results from the single-hit Schmidt hammer tests allowed for analysis of strength profiles along the rock walls (Figure 5). Average rebound values were assigned every 0.5 m up-unit starting from the trail or stream channel to a point past the carving or the extent of reach. From the strength profiles, segments of the same lithologic unit exhibited vertical differences in compressive strength based on location from the active stream channel or trail (Table 4). The location of the carving with respect to proximity to active foot travel or stream water interaction resulted in similarities in increased bedrock erosion potential. Large deviation values were also considered when describing a canyon's overall erodibility in context with supporting data.

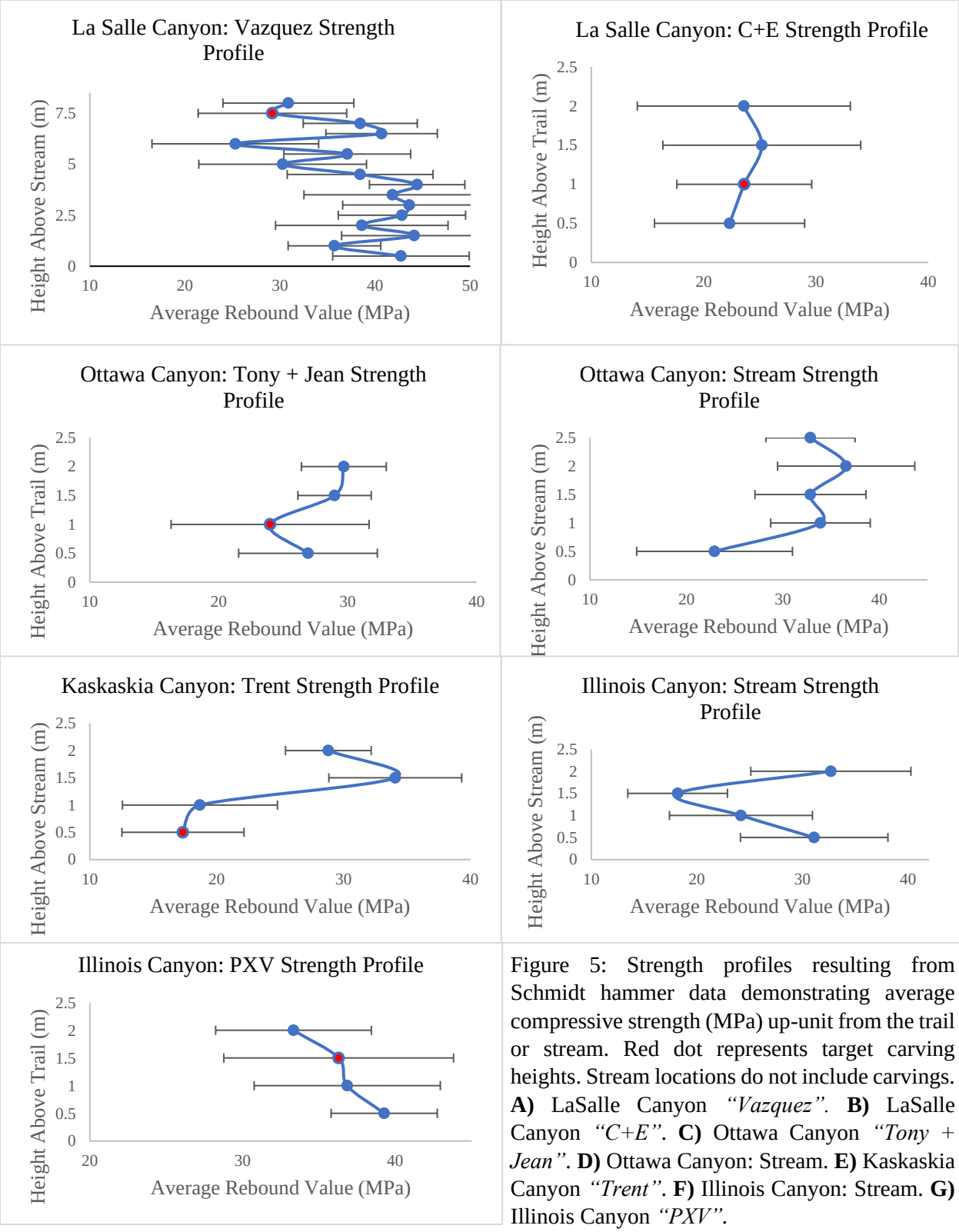

Figure 5: Strength profiles resulting from Schmidt hammer data demonstrating average compressive strength (MPa) up-unit from the trail or stream. Red dot represents target carving heights. Stream locations do not include carvings. **A)** LaSalle Canyon *"Vazquez"*. **B)** LaSalle Canyon *"C+E"*. **C)** Ottawa Canyon *"Tony + Jean"*. **D)** Ottawa Canyon: Stream. **E)** Kaskaskia Canyon *"Trent"*. **F)** Illinois Canyon: Stream. **G)** Illinois Canyon *"PXV"*.

Table 4: Results from Schmidt hammer strength profiles in Figure 5. Carving and stream locations are divided into sections to observe water influence and compare similar rebound strengths with contour weathering rates.

Schmidt Hammer Results		
Unit Segment	**Average Rebound Strength (MPa)**	**Average Standard Deviation**
LaSalle Canyon (*Vazquez*)		
0m - 4.5m	41.36	7.16
4.5m - 8m	33.12	7.26
Total	37.76	7.20
Ottawa Canyon (*Tony + Jean*)		
0m - 1m	25.45	6.53
1m - 2m	29.34	3.07
Total	27.40	4.80
Ottawa Canyon (Stream)		
0m - 0.5m	22.92	8.08
0.5m - 2.5m	34.05	5.66
Total	31.82	6.15
Kaskaskia Canyon (*Trent*)		
0m - 1m	18.01	5.46
1 m - 2m	31.44	4.31
Total	24.73	4.88
Illinois Canyon (Stream)		
0m - 0.5m	31.12	6.99
0.5m - 1.5m	21.18	5.75
1.5m - 2m	32.70	7.59
Total	26.55	6.52
Illinois Canyon (*PXV*)		
0m - 1m	38.07	4.79
1m - 2m	34.82	6.31
Total	36.45	5.55

Rock walls with their base at the stream channel showed more variability in rock strength than rock walls elevated above the stream valley floor. Observations from the Schmidt hammer test revealed distinct differences in strength up-unit at LaSalle (*Vazquez*) and Kaskaskia (*Trent*) Canyon test sites, which are both positioned close to the active stream channel. In contrast, the Ottawa (*Tony + Jean*) and Illinois (*PXV*) Canyon measurements were positioned far from water influence and exhibited smaller deviations. After identifying where the carving occurred within the strength profiles (Figure 5), it was noted that the carvings are similarly created in rock surfaces that were relatively weaker than the local surroundings. LaSalle Canyon (29.20 MPa), Ottawa Canyon (23.98 MPa), Kaskaskia Canyon (17.34 MPa), and Illinois Canyon (36.30 MPa) carvings all were created in sections of the

unit that are weaker than the overall average compressive strength of the profile. All measurements were executed on stable, intact bedrock to try to limit variability based on potential local differences in rock surfaces. Kaskaskia Canyon did have lichen and moss cover at the surface, potentially influencing the rebound values at that location.

Table 5: Summary of complied Schmidt hammer data by canyon found in Table 4.

Schmidt Hammer Result Comparison		
Canyon	**Average Rebound Strength (MPa)**	**Average Standard Deviation**
LaSalle	37.76	7.20
Ottawa	29.61	5.47
Kaskaskia	24.73	4.88
Illinois	31.50	6.03

An overall comparison of results from the 25 single-hit method at each carving provided an average rebound range of 37.76 MPa to 24.73 MPa (Table 5). LaSalle Canyon exhibited the highest rebound value at 37.76 MPa while Kaskaskia Canyon has the lowest, 24.73 MPa. Similarly, La Salle Canyon also produced the highest variation across the unit (±7.20 MPa) while Kaskaskia produced the lowest variation (±4.88 MPa). Further analysis will compare contour gauge profile erosion rates to the associated bedrock compressive strengths.

Petrographic Analysis

The thin section analysis of each canyon resulted in a range of grain, cement, and pore space values representing the conditions at the bedrock surface. Across the four canyons, grain percentages ranged from 73% to 83%, pore space percentages ranged from 5% to 15%, and cement percentages ranged from 5% to 22%. These ranges were comparable with porosity values seen in previous work by Haimson & Klaetsch (2007). The low calculated percent cement values provide beneficial information on the role of case hardening on these surfaces.

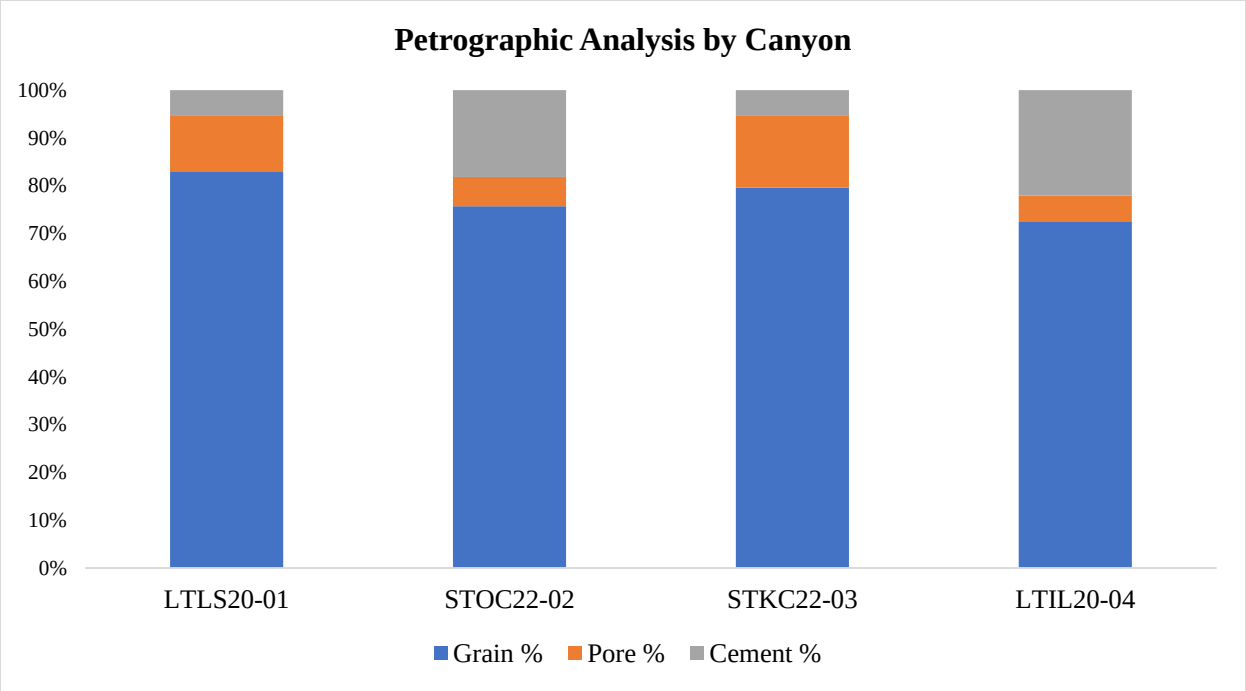

Figure 6: Graph representing petrographic analysis of each canyon by percent grains, pore space, and cement. LaSalle Canyon (LTLS20-01), Ottawa Canyon (STOC22-02), Kaskaskia Canyon (STKC22-03), and Illinois Canyon (LTIL20-04).

Figure 6 illustrates that sandstone samples in LaSalle and Kaskaskia Canyons contain relatively low amounts of cement at the surface (~5%), with a larger percentages of pore space and grains. Ottawa and Illinois Canyon samples have higher amounts of cement at the surface (20%) resulting in lower percentages of pore space. Comparing the percent cement in each canyon with respective average rock strength and erosion rates will be discussed to provide conclusions to the process of artificial degradation through the removal of surficial bedrock grains on the canyon wall.

LiDAR Analysis

The 3D LiDAR scans collected in each canyon were processed within the 3D Scanner app and exported into CloudCompare. Within CloudCompare, scans were aligned using the oldest scan, 11/8/22, as the reference and the latest scan, 1/28/23, as the compared. By using the November 2022 scan as a baseline, comparisons between the winter months of November and January can be described. Within CloudCompare the two scans were aligned by picking at least four points and once overlapped, the software calculated the root mean square error (RMS) of the alignment. The RMS was recorded for each scan and can be found in Table 6.

Table 6: Results from CloudCompare point-picking alignment tool. RMS (m) provided by scan alignment algorithm and converted to error (mm). Green shading represents good alignment and red shading represents poor alignment. Illinois Canyon produced the highest RMS error, valued at ±19 mm, whereas Ottawa Canyon showed the lowest error, ±6.7. All RMS errors are considered when describing scan technique and data limitations.

Scan Alignment Error			
Canyon	**Carving Name**	**RMS (m)**	**Error (mm)**
LaSalle	Vazquez	0.00889539	±8.8
Ottawa	Tony + Jean	0.00671077	±6.7
Kaskaskia	Trent	0.00920499	±9.2
Illinois	PXV	0.0190153	±19

As a rule, the alignment error or RMS error should equal or be greater than the accuracy of the scanner used to scan. An RMS value of 3 to 6 mm should be the minimum, if working with modern scanners. Since the overlap measurements are often imprecise, the alignment RMS is generally above 6 mm depending on the geometry of the environment. For exterior scans, an RMS error that is below 15 mm should indicate good alignment. In general, if the environment contains a lot of smooth surfaces and the alignment between two clouds is very good, then the RMS error is 6 mm or even lower. However, for scans that contain complex geometry with rough surfaces,

such as vegetation, the RMS error will be higher since the overlapping points may not always occupy the same location (Ahmad Fuad et al., 2018).

Scans produced from CloudCompare show changes represented by color. Cloud to cloud (C2C) absolute distance was calculated from the alignment and plotted against a red-white-blue color scale, chosen here to show discrepancies along the *z*-axis (Figures 7-10). Red signifies areas of accumulation from precipitation, sediment buildup, and increases in vegetation. Blue describes areas of weathering or erosion from natural or artificial influence as well as potential vegetation loss. White is shown as areas where little to no change can be detected from the scan resolution. Histogram visualizations are also shown (Figure 11), highlighting the localized differences between change within each of the canyons. C2C absolute distances (z) here rely on the resolution of the original scans regarding point-cloud size.

From the LiDAR scans, three of the outcrops showed more areas of positive change (LaSalle, Ottawa, and Illinois Canyon) and only one showed widespread negative change (Kaskaskia Canyon). All scans did, however, contain areas of white indicating no change occurred or could be detected. Kaskaskia Canyon proved to have the largest C2C absolute distance (z) range of values from 0.0138 to -0.0551 m while LaSalle Canyon had the smallest range from 0.0196 to -0.0087 m. Areas of over or under hanging rock shade the targeted surfaces and influenced the results from LiDAR analysis and negate any final conclusions.

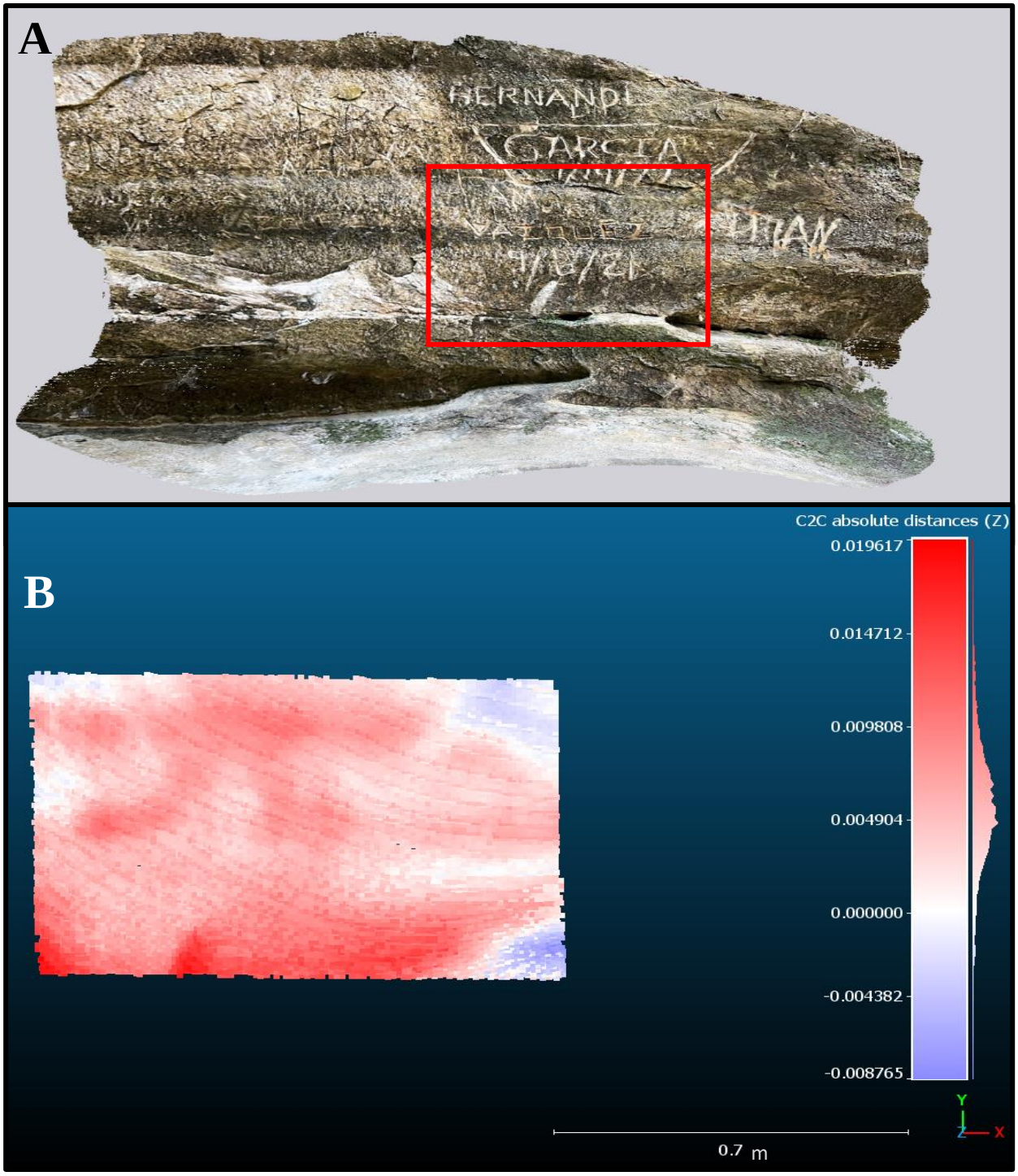

Figure 7: LaSalle Canyon *"Vazquez"* 3D CloudCompare comparison scan. **A)** Original point cloud scan taken from the 3D Scanner App. Red box highlights the targeted carved surface and rough dimensions of segmented CloudCompare scan. **B)** Processed difference comparison from November 22' to January 23'.

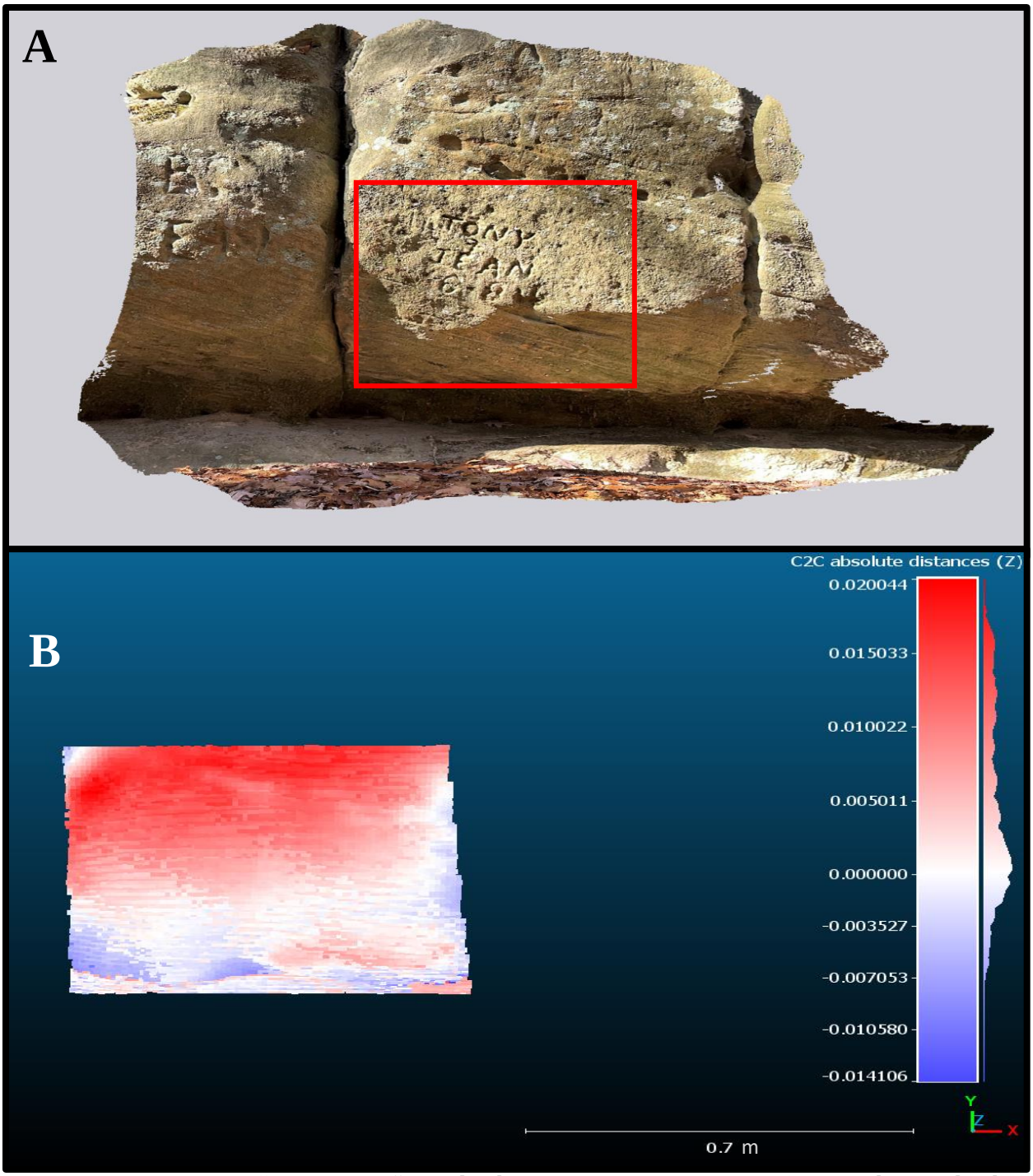

Figure 8: Ottawa Canyon *"Tony + Jean"* 3D CloudCompare comparison scan. **A)** Original point cloud scan taken from the 3D Scanner App. Red box highlights the targeted carved surface and rough dimensions of segmented CloudCompare scan. **B)** Processed difference comparison from November 22' to January 23'.

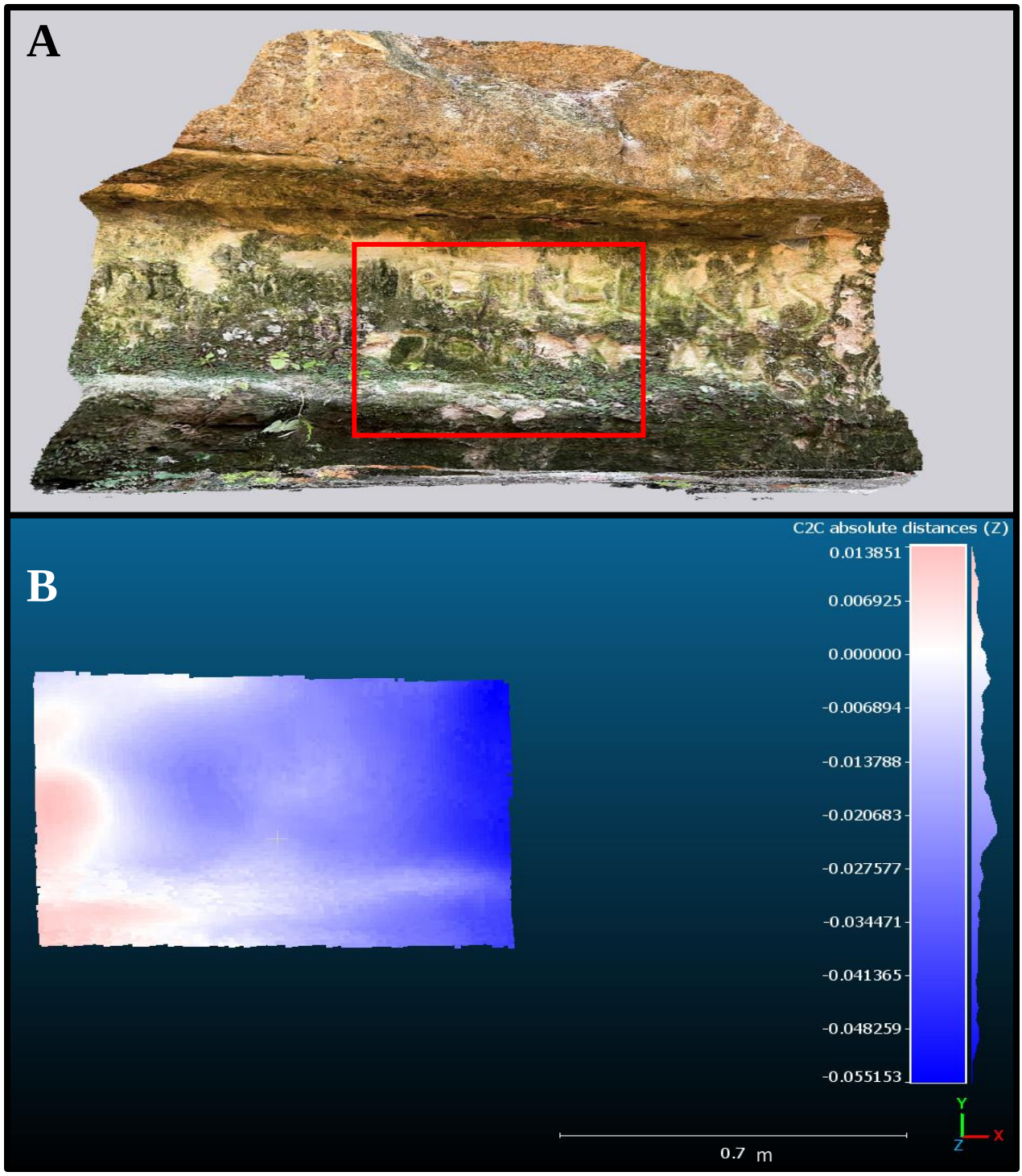

Figure 9: Kaskaskia Canyon *"Trent"* 3D CloudCompare comparison scan. **A)** Original point cloud scan taken from the 3D Scanner App. Red box highlights the targeted carved surface and rough dimensions of segmented CloudCompare scan. **B)** Processed difference comparison from November 22' to January 23'.

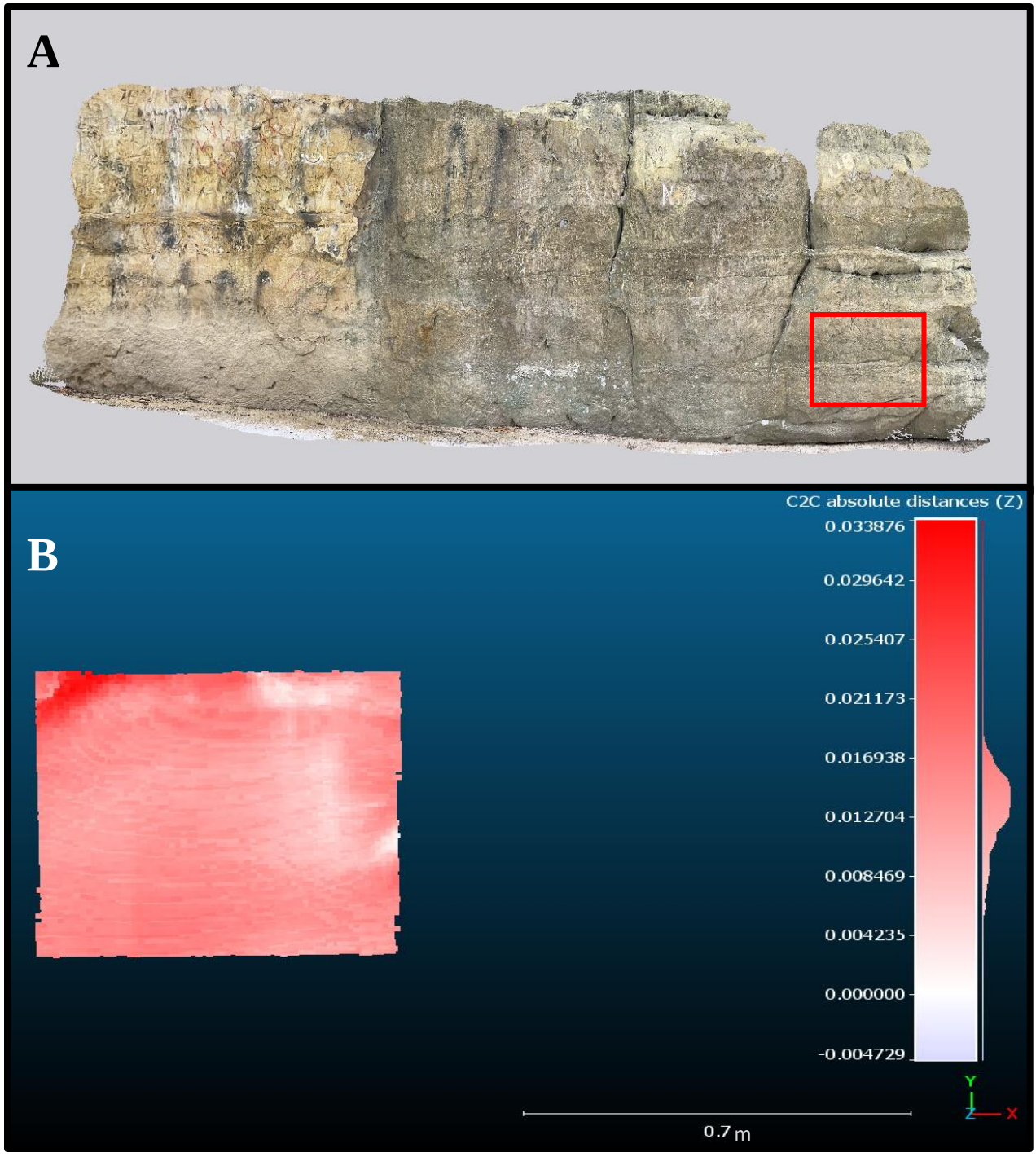

Figure 10: Illinois Canyon *"PXV"* 3D CloudCompare comparison scan. **A)** Original point cloud scan taken from the 3D Scanner App. Red box highlights the targeted carved surface and rough dimensions of segmented CloudCompare scan. **B)** Processed difference comparison from November 22' to January 23'.

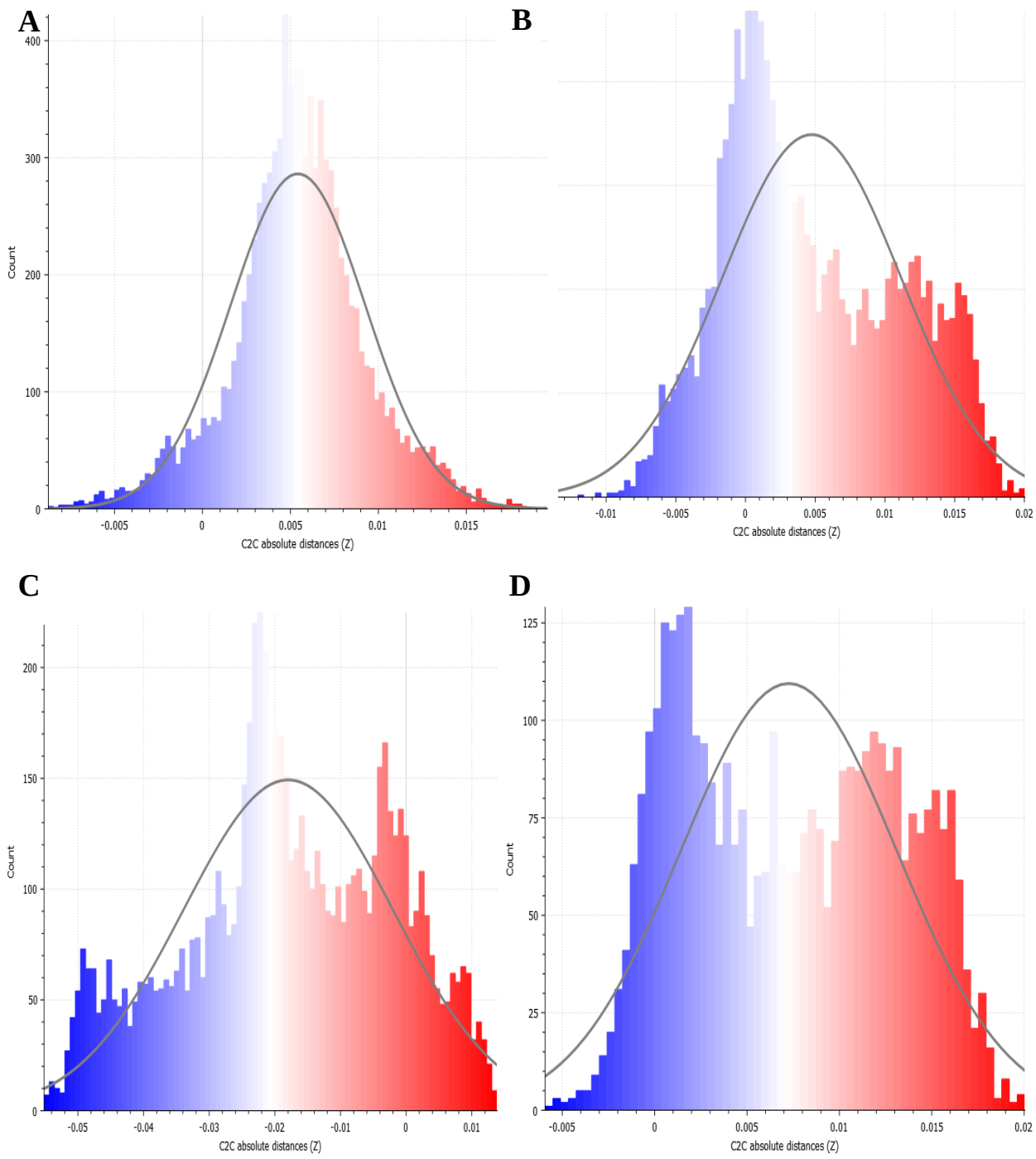

Figure 11: Histogram visualizations from resulting CloudCompare C2C distance (*z*) computations. **A)** LaSalle Canyon "*Vazquez*". **B)** Ottawa Canyon "*Tony + Jean*". **C)** Kaskaskia Canyon "*Trent*". **D)** Illinois Canyon "*PXV*". Gauss distribution curves are shown by the gray line and resulting Gauss mean and standard deviation values are listed above and in Table 7.

By utilizing the histogram function tool within CloudCompare, statistical analysis calculations were completed, and distributions were assigned. Using the Gaussian Distribution function allowed further explanation of results provided by C2C computation. Distribution analysis provided results for the Gaussian mean, standard deviation, the Chi2 distance and scalar field RMS of each canyon (Table 7). The Chi2 distance gives an evaluation of the fitting process quality: the greater the value the less the local distribution is likely to follow the tested one. LaSalle Canyon has the greatest "best fit", given by the Chi2 distance, whereas Illinois Canyon shows the least "best fit" of all the scans.

Analysis of the histogram statistical results also takes into consideration the initial alignment error given in Table 6. Results of the computation produce the final scalar field RMS error (m) given to calculate the total range of gain or loss on that surface (mm).

Table 7: Resulting statistical analysis values of the C2C computation from the associated histogram values. Gaussian mean (m) and scalar field RMS (m) are converted to mm and calculated into total difference (mm) and total range values (mm) used for further discussion.

Statistical Distribution Analysis of C2C Computation							
Canyon	**Carving Name**	**Gauss Mean (m)**	**Standard Deviation**	**Chi2 Distance**	**Scalar Field RMS (m)**	**Total Difference (mm)**	**Total Range (mm)**
La Salle	Vazquez	0.005426	0.003797	736.6	0.00662	5.4 ± 6.6	-1.2 – 12.0
Ottawa	Tony + Jean	0.004725	0.006322	1355.8	0.00789	4.7 ± 7.9	-3.2 - 12.3
Kaskaskia	Trent	-0.017998	0.015782	1148.8	0.0239	-18.0 ± 23.9	-41.9 - 5.9
Illinois	PXV	0.007526	0.005766	1817.1	0.0139	7.5 ± 13.9	-6.4 – 21.4

CHAPTER V: DISCUSSION

Contour Gage Analysis

Contour gauge profiles were used to determine the influence carving has on natural erosion. Average change calculated by contour gauge profiles from all control and carving data exhibit a range of erosivity across the canyons (Figure 12). The cumulative average per canyon showed both Kaskaskia and LaSalle Canyon having the same amount of change during the study period, at 1.8 ± 0.9 mm. This difference is the highest change seen within the four canyons, while Ottawa Canyon only produced a total of 1.0 ± 0.5 mm of erosion, resulting in the lowest total change. Illinois Canyon, also, showed a similar cumulative change like LaSalle and Kaskaskia, at 1.7 ± 0.8 mm. With a total difference of 0.8 ± 0.4 mm between the four canyons, this discrepancy could be contributed to internal influences (rock strength, stratigraphic position, sun exposure, etc.) or external influences (biological activity, climate, humans, etc.) affecting erosion within individual

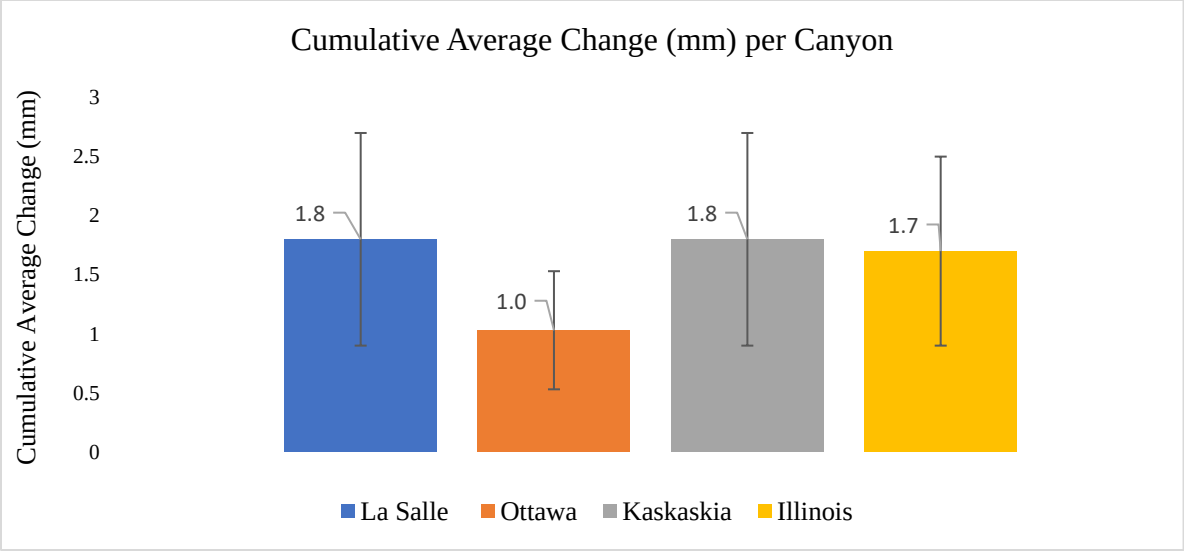

Figure 12: Average erosion by canyon. LaSalle and Ottawa Canyon include multiple carving and control erosion values averaged together for an overall erosivity by canyon. Error bars represent variability within the calculated change values.

canyons. These data, however, are the total of all contour data collected by canyon and only address the overall erosivity of the bedrock.

Previous work in Starved Rock measured erosion at canyon heads within the park and found an average erosion rate of 20 mm/yr, with a range of 10-50 mm/yr (Irvine, 2001). The results presented in Irvine (2001), however, tracked erosion along the longitudinal and cross-profiles of the canyons, while this study focused on localized changes to bedrock surfaces. Our work resulted in a lower average erosion of 1.6 ± 0.8 mm throughout the four canyons than seen by Irvine (2001). We do see similar processes affecting erosion within the canyons like those explained in Irvine (2001), but evidence in the comparisons of carving to control erosion rates will answer our research questions in determining the human influence within the park.

We hypothesized that carvings would influence natural erosion processes occurring on bedrock walls. The variations between carving profiles and control profiles (Table 3), support our hypothesis. LaSalle Canyon's "*Vazquez (a-z)"* carving produced the largest difference between the carved and controlled surface, at a total of 2.2 ± 1.4 mm. Illinois Canyon's "*PXV"* carving follows close behind with a 0.7 ± 0.4 mm total difference. The smallest difference of 0.1 ± 0.1 mm between the carved and unaltered surface was observed at Ottawa Canyon's *Tony + Jean* carving site. La Salle Canyon's "*C+E"* carving, Ottawa Canyon's "*Tony + Jean"* carving and Kaskaskia Canyon's "*Trent"* carvings all indicated the least change between the carvings and controls. The variability in the amount of change between the carvings and control profiles suggest that carving increases the roughness on the bedrock surface and thus influences its resistance to weathering. By scraping off small sections of the bedrock, fresh, weakly cemented grains were exposed to

increases in physical, biological, and chemical weathering. This process of removing surficial grains caused a breakdown in the protective coating of the bedrock and an increase in exposed fresh surface area, prompting increased erosion.

More frequent carvings and year-round, easy access to carving sites in LaSalle and Ottawa Canyon allowed for more opportunities for data collection and further exploration of variability within the two canyons. LaSalle Canyon's *Vazquez* carving resulted in a 2.8 ± 1.6 mm difference, but "*C+E"* only changed 1.4 ± 0.6 mm. Similarly, in Ottawa Canyon, "*T+J"* had a difference of 1.3 ± 0.6 mm, while "*Tony + Jean"* only resulted in a 1.0 ± 0.5 mm change. This suggests there can be a small range of erosion rates seen within individual canyons related to the origin of the carving and stabilization of these carved surfaces over time. The "*Vazquez"* and "*T+J"* carvings were both located near actively flowing water in the channels. The "*C+E"* and "*Tony + Jean"* carvings were both positioned along trails, but high enough above the stream channels that they

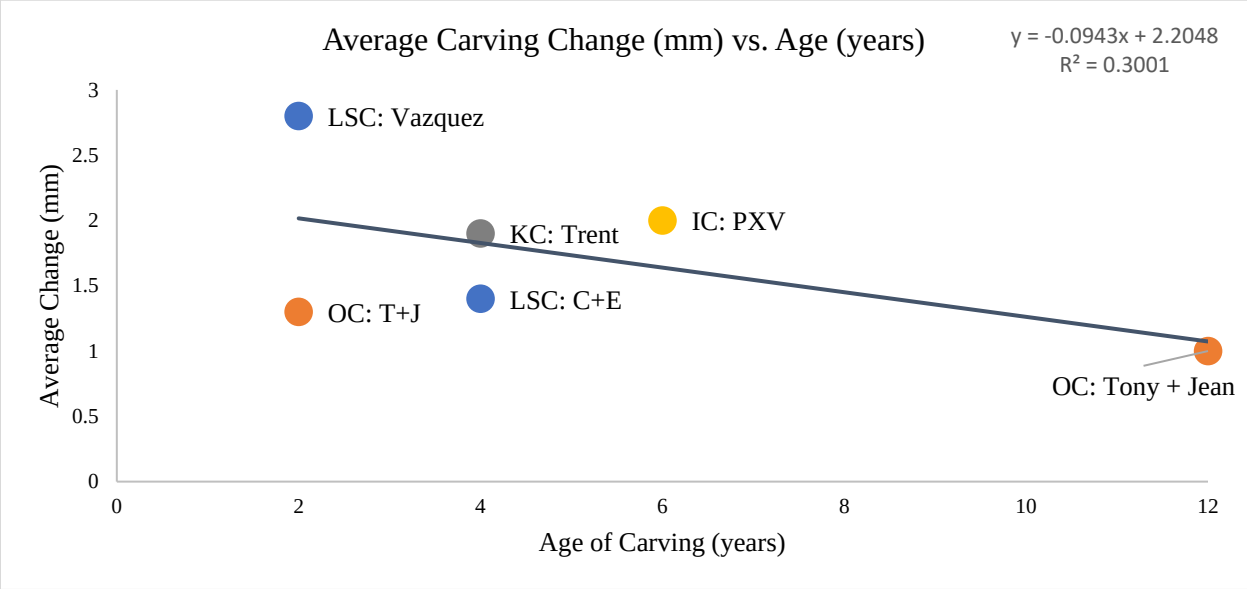

Figure 13: Results of contour gauge average carving change (mm) compared with relative age of each carving. Equation and R^2 values given for correlation.

were not influenced by actively flowing or splashing water. The age of the carvings could, also, be a factor in the variability seen within the canyons.

Some of the targeted carvings provided a date when it was created by the authors. We know when LaSalle Canyon's "*Vazquez"*, Ottawa Canyon's "*Tony+ Jean*", Ottawa Canyon's "*T+J"* and Kaskaskia Canyon's "*Trent"* carvings were created, based on inscriptions of dates next to the carving. We also know when LaSalle Canyon's "*C+E"* carving and Illinois Canyon's "*PXV"* carving were created. Based on data provided by past researchers, we can restrict the date of the carvings to prior to when prior research was initiated. Apart from Ottawa Canyon's *"T+J"* carving, the relationship between the age of the carvings and their respective erosion rates provided in Figure 13 indicate that over time these carved surfaces will stabilize and develop a higher resistance to weathering than areas where the carving recently occurred. Stabilization involves the process of reintroducing case hardening to the fresh surface over time, sealing up those weakly cemented grains to maintain the structural integrity of the bedrock.

Temporal and spatial variability among the contour erosion rates also can be influenced by seasonal fluctuations of temperature and precipitation. When separating the contour data taken in cold months (January 2022, March 2022, November 2022, and January 2023) and warm months (May 2022, July 2022, September 2022) it is evident that erosion can occur more prominently in both colder and warmer conditions due to different biological, solar, and water influences occurring at each site (Figure 4). Mechanisms of freeze-thaw could provide answers to why we see an increase in the cold months in some areas; and sources of biologic activity that thrive in warm conditions may provide protection for some of these surfaces during the summer. In

Kaskaskia Canyon, carvings are in areas close to water sources and heavily shaded by trees and overhangs, causing intensive moss and lichen cover at the bedrock surface. The role of biological activity provides slight protection against erosion when warm weather permits the creation of such colonies, but during cold months, they die off and expose the surface to erosive processes. During the summer months if this moss or lichen were to be disturbed prematurely and fall off the bedrock surface, the roots remove microscopic sand grains from the surface, prompting slight increases in erosion. Biological activity can have both a negative and positive effect on these rock surfaces.

Rock Strength Analysis

Schmidt hammer tests were conducted using the 25 single-hit method on targeted outcrops within the park. Results from the tests show rebound values ranging from 37.76-24.73 MPa with respective deviation values of 7.20-4.88 MPa. The lowest rebound values are in Kaskaskia Canyon (24.73 MPa), followed by Ottawa Canyon (29.60 MPa). The highest rebound values are in LaSalle Canyon (37.76 MPa) and Illinois Canyon (31.50 MPa) (Table 5).

Overall, the high standard deviation of rock strength values taken along the bedrock wall profiles indicate that rock strengths are relatively similar both on the valley floor or elevated above the active stream channel. We did note, however, that the profiles on the valley floor at the level of the active stream channel showed higher variability at their base than the elevated segment above (Figure 5). Profiles taken at the active stream channel in Ottawa and Kaskaskia Canyon (Figure 5D and 5E) show weaker bedrock at the base, where erosion by crumbling undercut bedrock was observed. Bedrock was stronger in the upper segment elevated above the valley floor. Profiles taken at the active stream channel in LaSalle and Illinois Canyon (Figure 5A and 5F) show

stronger bedrock at the base, where water actively flows, followed by weaker bedrock up-segment. Regardless, all target carving heights were coincidently located in weaker units of the profiles.

These observations support the expectation that weathering varies across bedrock-floored channels, but the data do not reveal a pattern of increasing erodibility with greater height above the active channel as previously concluded by Shobe et al., 2017. We observed evidence of mineralization filling open pore spaces on the surface of the bedrock where active water flowed, producing stronger bedrock as seen in the LaSalle Canyon "*Vazquez*" strength profile. Alternatively, processes occurring at the active stream channel caused undercutting of the bedrock through abrasive mechanical weathering. Evidence of this exists at target rock strength locations on the Ottawa Canyon "Stream", Kaskaskia Canyon "*Trent*", and Illinois Canyon "Stream" profiles where the first 0.5-1.0 m of the rock strength profile exhibited weaker bedrock compared to the upper segment. Relating the percentage of cement measured in each thin section by canyon could determine if there is a correlation between rock strength and our calculated contour erosion rates.

Petrographic Analysis

Conducting petrographic analysis on boulders taken from rock falls within each canyon allowed for an investigation of the role of case hardening on these surfaces. Results from the thin section analysis showed spatial variability of the characteristics of the St. Peter Sandstone throughout the park. The presence of cement within the top 5 mm of the four samples ranges from as little as 5%, up to 20%. This discrepancy could relate to the variability seen within our measured rock strength values and differences within the canyon control erosion rates.

The presence of cement on the bedrock surface provides protection against erosion (Dorn et al., 2017). However, eventually, case-hardened crusts would exfoliate, exposing the core-softened interior to rapid weathering again (Pope et al., 2002). This natural cycle of detachment is accelerated when the case-hardened grains are removed from the bedrock surface through carving. This evidence suggests that the St. Peter Sandstone is variable over a small spatial area and any disturbance on the bedrock surface could result in removal of the already little to no cement and prompt increases in erosion.

LiDAR Analysis

By utilizing a new form of 3D LiDAR scan technology, we studied the capability to determine small-scale geoscience changes along a surface. Initial alignment error provided in Table 6, shows Illinois Canyon's "*PXV"* carving alignment error was outside the scope of negligible error (>15 mm), whereas the rest of the canyons remained consistent with good alignment (<15 mm). Alignment error, however, is carried throughout the analysis into the Gaussian distribution statistical analysis which will be used for concluding the accuracy and implications of hand-held LiDAR compatibility.

Results of the final computation of each scan produced a wide range of difference values (Table 7). LaSalle Canyon had a mean difference of +5.4 mm with the lowest deviation value of ±6.6 mm, producing a range of -1.2 mm to 12.0 mm total difference. Ottawa Canyon also resulted in a similar mean difference of +4.7 mm with a deviation of ±7.9 mm, producing a range of -3.2 mm to 12.3 mm total difference. Kaskaskia and Illinois Canyon both resulted in large ranges of total differences seen on the surfaces. Kaskaskia Canyon resulted in a loss at the surface of -18.0

mm with a deviation of ±23.9 mm, creating the largest range of -41.9 mm to 5.9 mm. Illinois Canyon carried the highest alignment RMS error (+19 mm) throughout the statistical distribution analysis, but was not the highest final deviation value. Illinois Canyon resulted in a +7.5 mm change with a deviation of ±13.9 mm, causing the total range of difference between -6.4 mm and 21.4 mm.

With high deviation values and large total difference ranges we conclude that our results are not consistent with our research objectives and will not be used for further comparisons. Scan technique, lighting conditions, vegetation and precipitation are all factors regarding our final error and implications for this study.

Comparison Analysis

Schmidt hammer tests and contour gauge profiles were compared to determine the overall influence of carving on natural erosion; LiDAR results are not included based on accuracy. From Figure 14, we can see there is a negative correlation between rock strength (MPa) and difference values between the control profiles, but the calculated carving difference values do not follow a similar pattern. This distinct separation between the carvings and controls indicates this relationship between rock strength and erosion rate is disrupted when carving on the surface occurs. This evidence is proof that the role of case hardening and the consequences of removing the surficial grains has the largest impact on increasing erosion potential from human interaction.

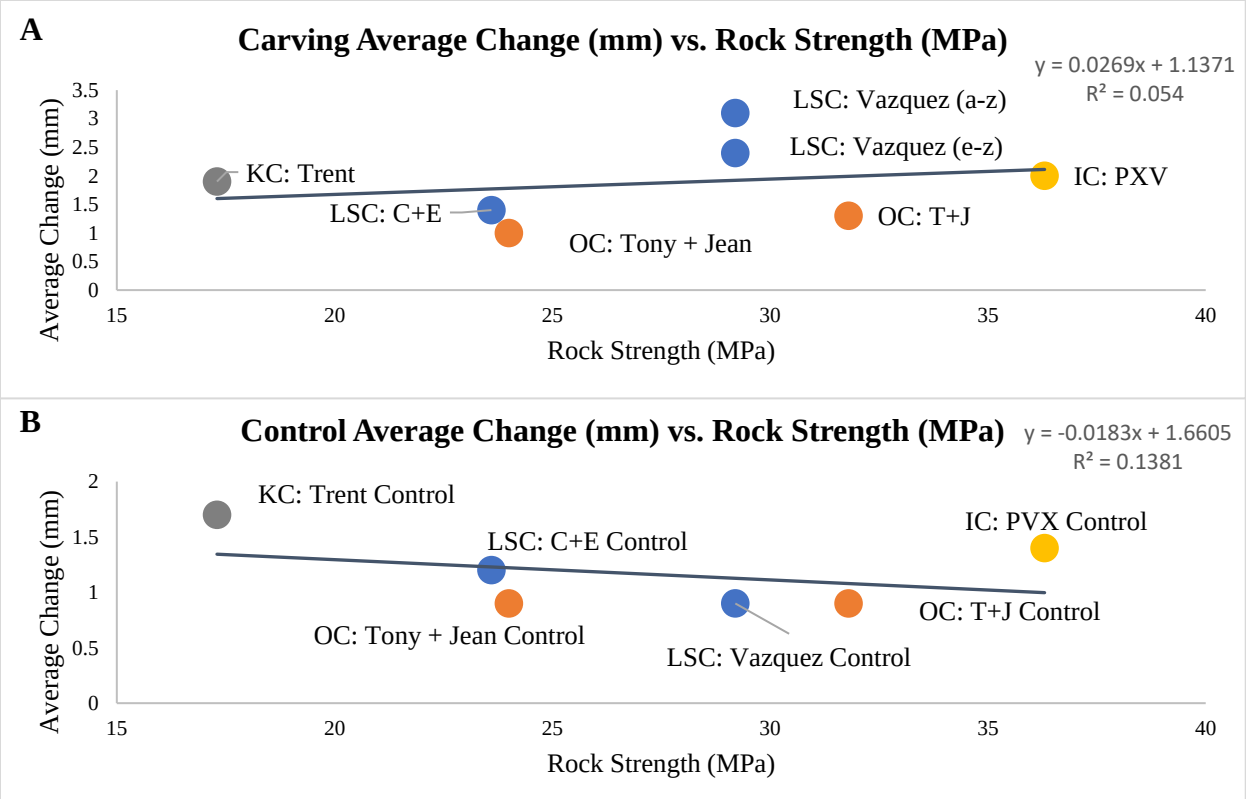

Figure 14: Graph representing the relationship between average change and rock strength. **A)** Carving average change and rock strength. **B)** Control average change and rock strength. A negative correlation is shown between the control **(B)**, confirming weaker rock experiences increases in erosion within our study period. A positive relationship between the carving's average change and rock strength **(A)** are seen, concluding carving does influence the bedrock's ability to resist weathering. Equation and R^2 values given for correlation.

From Figure 15, a negative correlation is shown between the comparison of our average calculated canyon erosion rates to the measured percent cement from our thin sections. This relationship thus explains the importance of the presence of cement at the surface of these outcrops in its ability to resist weathering. Case hardening within the park is evident in the thin sections and influences the potential for change on the rock surface. While the case hardening offers short-term resistance to erosion, over time, this hardened bedrock's surface may detach as a solid sheet from the rest of the sandstone block holding it as observed on some rock surfaces and canyon walls in

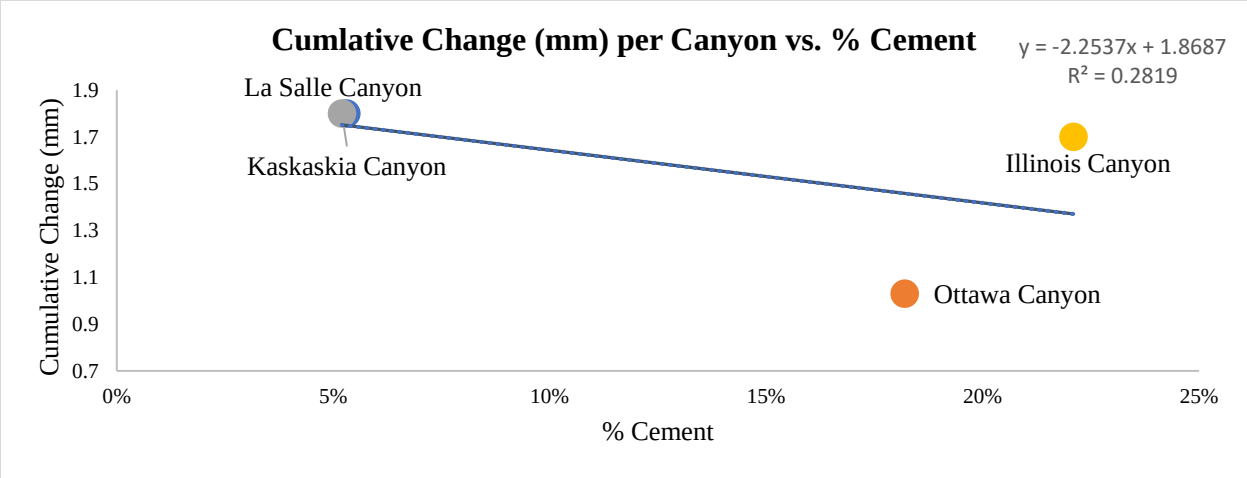

Figure 15: Graph representing the comparison of the total cumulative change (mm) by canyon versus percent cement calculated from thin section analysis. Equation and R^2 values given for correlation.

the park (Include a photo example that you had in the presentation as Figure 16. Consequently, an abrupt backward recession of the bedrock surface will occur and expose a fresh (un-weathered) surface ready for further weathering (roughening and recession) (Turkington & Paradise, 2005). When the hardened surface is breached, rapid erosion of the underlying, newly exposed grains will occur. Evidence in the removal of case hardening processes is prominent in the action of carving, but further investigation with more dated examples of carvings could offer an in-depth evaluation of the re-stabilization of these surfaces with time. A study done by Turkington & Paradise (2005) found that after the weathered material erodes away, the surface can restabilize and begin to case harden again. Proof of this re-stabilization is found at our Ottawa Canyon "*Tony + Jean*" carving, where the change on the carved surface and the control were similar. The removal of case hardening when a carving is created accelerates erosion, as observed on LaSalle Canyon's "*Vazquez*" carving, but the surface stabilizes over an extended period. This process of re-

stabilization aids in the longevity of these outcrops, but with intensive tourism, short-term erosivity of the park could become a concern.

Limitations and Future Work

Throughout the study, some complications arose with the methodology and analysis of the results. With the application of new LiDAR technology, only a few technical articles have been published concerning the use of these devices for fast, small-scale surveying (Teppati Losè et al., 2022). Techniques involving the use of the 3D Scanner App are restricted to the size and shape of the scan (Teppati Losè et al., 2022), reflectance (Mikita et al., 2022), surface texture (Luetzenburg et al., 2021), ambient lighting (Łabędź et al., 2022), the distance between object and scanner (Mikita et al., 2022), scanning strategy, and movements (Costantino et al., 2021). All these factors combined can influence the quality of the scan and limit conclusions. Over and under hangs which shade the surface are shown to affect the statical analysis results (Łabędź et al., 2022). Future work regarding this software involves a consistent routine set of techniques which will be utilized throughout all scanning activities to retain scan accuracy. Recommendations of scan techniques would involve a preliminary set-up of tape, marker, or chalk on the surface to have reference points for scan alignments as well as a line or mark representing the scan distance from the object. Stationary tripods help prevent any human error of walking speed or changing scan heights while also being able to change orientation without affecting the scan. With continued utilization of new technology, future research regarding the small-scale capabilities of Apple's © iPhone 13 Pro LiDAR will be developed and allow for more applications throughout different fields.

Future work regarding Starved Rock State Park should involve a more intensive study of human influences seen within the park. With this area receiving more visitors annually, it is important for park officials to maintain this State beauty. This study, however, only captured small scale erosion across one year, which can be difficult to impossible to extrapolate over longer time periods. This work would benefit educators at the park if it were extended to a 5-year study. Human impacts on erosion rates within the park do not stop at the carvings, but also extend to wear and tear on trails, off-trail paths, and spray-paint graffiti on signs and bedrock. Further research into the other factors affecting erosion within the park would allow for a more precise conclusion of the overall human impact of the park.

CHAPTER VI: CONCLUSION

From the methods applied in this study, the contour gauge, Schmidt hammer, and petrographic analysis data provided adequate information for comparisons of human-induced erosion versus natural erosion. Since the resolution was low across the large area scanned with the iPhone 13 Pro scanner and lighting variables could not be controlled or held constant, large errors were introduced in the LiDAR analyses and restricted discussion of final conclusions from this method. However, the evidence presented in this paper proves humans do influence the erosion of bedrock on a millimeter scale within the park, confirming our hypothesis. This human interaction proves to degrade the park at a faster rate than natural erosion through the breakdown of case hardening. The longevity of these surfaces over time is maintained as natural processes reintroduce case hardening after carving occurs. Further work observing human interactions within the park could offer valuable information to the future evolution of these fragile canyon walls and identify any long-term effects that lay out of the scope of this study.

The purpose of the research was to identify and observe anthropogenic impacts on this state park. By creating this awareness, park officials now have the knowledge to inform visitors to become more conscious about how they can respect the park and others. The need for protection is a pillar for the continued existence of these parks and as tourism increases, the short-term repercussions become evident. By limiting the consequences of human-induced erosion from these outcrops, the longevity of the park will remain, while future visitors will be able to fully appreciate the natural beauty of the park. Identifying the short-term human impact on geological structures proved valuable in gaining an overview of our compounding influence within the park.

REFERENCES

Adams, S. L., Maclaughlin, M. M., Berry, K. G., Mccormick, M. L., Berry, S. M., Mcgough, M., & Hudyma, N. (2014). Three-Dimensional Roughness Characterization of Rock Joints using Laser Scanning and Wind Diagrams. In *Mechanics/Geomechanics Symposium*.

Ahmad Fuad, N., Yusoff, A. R., Ismail, Z., & Majid, Z. (2018). Comparing the performance of point cloud registration methods for landslide monitoring using mobile laser scanning data. *ISPRS - International Archives of the Photogrammetry Remote Sensing and Spatial Information Sciences*, *XLII-4/W9*, 11–21. https://doi.org/10.5194/isprs-archives-xlii-4-w9-11-2018

Ancin-Murguzur, F. J., Munoz, L., Monz, C., & Hausner, V. H. (2020). Drones as a tool to monitor human impacts and vegetation changes in parks and protected areas. *Remote Sensing in Ecology and Conservation*, *6*(1), 105–113. https://doi.org/10.1002/rse2.127

Aydin, A., & Basu, A. (2005). The Schmidt hammer in rock material characterization. *Engineering Geology*, *81*(1), 1–14. https://doi.org/10.1016/j.enggeo.2005.06.006

Aydin, O., & Yassikaya, M. Y. (2022). Validity and reliability analysis of the PlotDigitizer software program for data extraction from single-case graphs. *Perspectives on Behavior Science*, *45*(1), 239–257. https://doi.org/10.1007/s40614-021-00284-0

Carter, N. E. A., & Viles, H. A. (2005). Bioprotection explored: the story of a little known earth surface process. *Geomorphology (Amsterdam, Netherlands)*, *67*(3–4), 273–281. https://doi.org/10.1016/j.geomorph.2004.10.004

Černá, B., & Engel, Z. (2011). Surface and sub-surface Schmidt hammer rebound value variation for a granite outcrop. *Earth Surface Processes and Landforms*, *36*(2), 170–179. https://doi.org/10.1002/esp.2029

Chang, C., Zoback, M. D., & Khaksar, A. (2006). Empirical relations between rock strength and physical properties in sedimentary rocks. *Journal of Petroleum Science & Engineering*, *51*(3–4), 223–237. https://doi.org/10.1016/j.petrol.2006.01.003

Coombes, M. A., Viles, H. A., & Zhang, H. (2018). Thermal blanketing by ivy (Hedera helix L.) can protect building stone from damaging frosts. *Scientific Reports*, *8*(1), 9834. https://doi.org/10.1038/s41598-018-28276-2

Costantino, D., Vozza, G., Pepe, M., & Alfio, V. S. (2022). Smartphone LiDAR technologies for surveying and reality modelling in urban scenarios: Evaluation methods, performance and challenges. *Applied System Innovation*, *5*(4), 63. https://doi.org/10.3390/asi5040063

Davis, J.G. (2014). St. Peter Sandstone Mineral Resource Evaluation, Missouri, USA, in, Conway, F.M., ed., Proceedings of the 48th Annual Forum on the Geology of Industrial Minerals, Phoenix, Arizona, April 30 - May 4, 2012. Arizona Geological Survey Special Paper #9, Chapter 6, p. 1-7.

Dorn, R., Whitley, D., Cerveny, N., Gordon, S., Allen, C., & Gutbrod, E. (2008). The Rock Art Stability Index: A new strategy for maximizing the sustainability of Rock Art. Heritage & Society, 1(1), 37–70. https://doi.org/10.1179/hso.2008.1.1.37

Dorn, R. I., Mahaney, W. C., & Krinsley, D. H. (2017). Case hardening: Turning weathering rinds into protective shells. Elements, 13(3), 165–169. https://doi.org/10.2113/gselements.13.3.165

Drevon, D., Fursa, S. R., & Malcolm, A. L. (2017). Intercoder reliability and validity of WebPlotDigitizer in extracting graphed data. *Behavior Modification*, *41*(2), 323–339. doi:10.1177/0145445516673998

Favero-Longo, S. E., & Viles, H. A. (2020). A review of the nature, role and control of lithobionts on stone cultural heritage: weighing-up and managing biodeterioration and bioprotection. *World Journal of Microbiology and Biotechnology*, *36*(7), 100. https://doi.org/10.1007/s11274-020-02878-3

Gollob, C., Ritter, T., Kraßnitzer, R., Tockner, A., & Nothdurft, A. (2021). Measurement of forest inventory parameters with Apple iPad Pro and integrated LiDAR technology. *Remote Sensing*, *13*(16), 3129. https://doi.org/10.3390/rs13163129

Gordon, S. J., & Dorn, R. I. (2005). In situ weathering Rind Erosion. *Geomorphology*, *67*(1-2), 97–113. https://doi.org/10.1016/j.geomorph.2004.06.011

Haimson, B., & Klaetsch, A. (2007). Compaction bands and the formation of slot-shaped breakouts in St. Peter sandstone. *Geological Society Special Publication*, *284*(1), 89–105. https://doi.org/10.1144/sp284.7

Hoholick, J.D., Metarko, T.A., & Potter, P.E. (1984). Regional variations of porosity and cement; St. Peter and Mount Simon sandstones in Illinois Basin. *AAPG Bulletin, 68*, 753-764.

Huysken, K., Argyilan, E., & Votaw, R. (2016). Project-based field trips to the Starved Rock area for geoscience educators, northern Illinois. In Z. Lasemi & S. D. Elrick (Eds.), *Celebrating 50 Years of Geoscience in the Mid-Continent: Guidebook for the 50th Annual Meeting of the Geological Society of America North Central Section.*

Irvine, M. C. (2001). Sandstone Canyon Development in Starved Rock State Park [Ball State University]. http://liblink.bsu.edu/catkey/1222828

Kamh, G. M. E., & Koltuk, S. (2016). Micro-topographic and Geotechnical Investigations of sandstone Wall on Weathering Progress, Aachen City, Germany, case study. *Arabian Journal for Science and Engineering*, *41*(6), 2285–2294. https://doi.org/10.1007/s13369-015-1887-3

Laan, J. (2022). TrueDepth Scanning - Accurate small scans with the iPhone Infrared Depth Sensor. Retrieved January 23, 2023, from Laan.com website: https://labs.laan.com/casestudies/truedepth-3d-scanning-case-study

Łabędź, P., Skabek, K., Ozimek, P., Rola, D., Ozimek, A., & Ostrowska, K. (2022). Accuracy verification of surface models of architectural objects from the iPad LiDAR in the context of photogrammetry methods. *Sensors (Basel, Switzerland)*, *22*(21), 8504. https://doi.org/10.3390/s22218504

Luetzenburg, G., Kroon, A., & Bjørk, A. A. (2021). Evaluation of the apple iPhone 12 Pro LiDAR for an application in geosciences. *Scientific Reports*, *11*(1), 22221. https://doi.org/10.1038/s41598-021-01763-9

McCarroll, D., & Nesje, A. (2008). The vertical extent of ice sheets in Nordfjord, western Norway: measuring degree of rock surface weathering. *Boreas*, *22*(3), 255–265. doi:10.1111/j.1502-3885.1993.tb00185.x

Mikita, T., Krausková, D., Hrůza, P., Cibulka, M., & Patočka, Z. (2022). Forest road wearing course damage assessment possibilities with different types of laser scanning methods including new iPhone LiDAR scanning apps. *Forests*, *13*(11), 1763. https://doi.org/10.3390/f13111763

Montecillo, F. F. A. (2018). Starved Rock State Park faces overcrowding challenges. Retrieved February 8, 2023, from Illinois Public Media website: https://will.illinois.edu/21stshow/program/starved-rock-overcrowded

Nelson, R.S, Malone, DH., Jacobson, RJ., & Frankie, W.T. (1996). Guide to the Geology of Buffalo Rock and Matthiessen State Parks Area, La Salle County, Illinois. In *Illinois Geological Survey Field Trip Guidebook* (p. 56).

Pope, G. A., Meierding, T. C., & Paradise, T. R. (2002). Geomorphology's role in the study of weathering of Cultural Stone. Geomorphology, 47(2-4), 211–225. https://doi.org/10.1016/s0169-555x(02)00098-3

Rutte, M. M. (2018). Analysis of Short-term Erosion of the St. Peter Sandstone in La Salle County, Illinois [Illinois State University]. https://ir.library.illinoisstate.edu/etd/929

Shobe, C. M., Hancock, G. S., Eppes, M. C., & Small, E. E. (2017). Field evidence for the influence of weathering on rock erodibility and channel form in bedrock rivers: WEATHERING AND CHANNEL FORM IN BEDROCK RIVERS. *Earth Surface Processes and Landforms*, *42*(13), 1997–2012. doi:10.1002/esp.4163

Teppati Losè, L., Spreafico, A., Chiabrando, F., & Giulio Tonolo, F. (2022). Apple LiDAR sensor for 3D surveying: Tests and results in the cultural heritage domain. *Remote Sensing*, *14*(17), 4157. https://doi.org/10.3390/rs14174157

Turkington, A. V., & Paradise, T. R. (2005). Sandstone weathering: A century of research and Innovation. *Geomorphology, 67*(1-2), 229–253. https://doi.org/10.1016/j.geomorph.2004.09.028

Viles, H., Goudie, A., Grab, S., & Lalley, J. (2011). The use of the Schmidt Hammer and Equotip for rock hardness assessment in geomorphology and heritage science: a comparative analysis. *Earth Surface Processes and Landforms*, *36*(3), 320–333. doi:10.1002/esp.2040

Vogt, M., Rips, A., & Emmelmann, C. (2021). Comparison of iPad Pro®'s LiDAR and TrueDepth capabilities with an industrial 3D scanning solution. *Technologies*, *9*(2), 25. https://doi.org/10.3390/technologies9020025

Willems, B. A., Malone, D. H., & Pugin, A. (2007). Geologic characteristics of the central stretch of the Ticona Channel, north-central Illinois. *Environmental Geosciences*, *14*(3), 123–136. doi:10.1306/eg.05030606002

APPENDIX: CONTOUR PROFILES

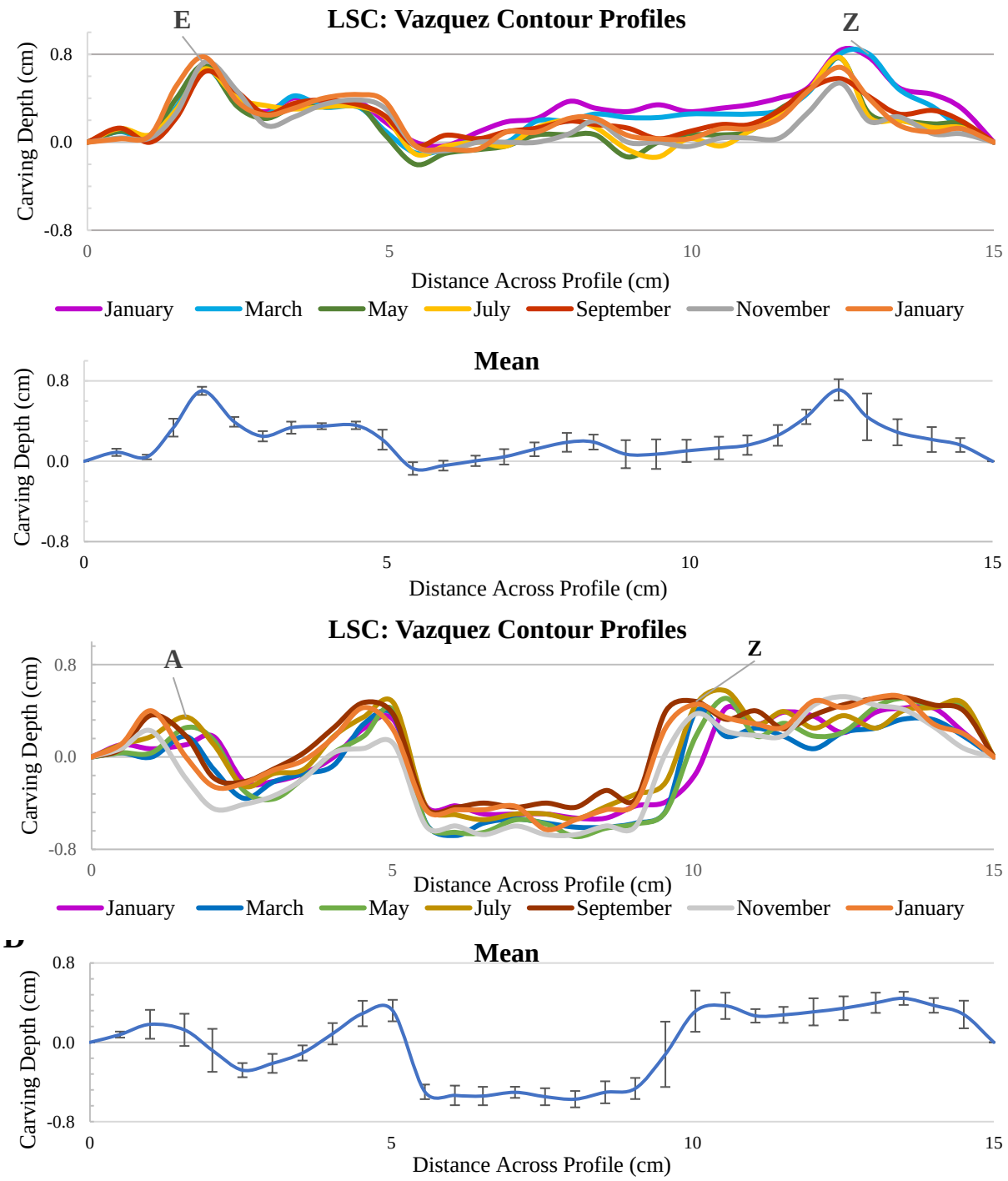

A1: LaSalle Canyon's "*Vazquez"* carving and respective mean profiles from January 22' to January 23'. **A) "***Vazquez"* (E-Z) profiles. **B) "***Vazquez"* (E-Z) mean profile. **C) "***Vazquez"* (A-Z) profiles. **D)** "*Vazquez"* (A-Z) mean profile.

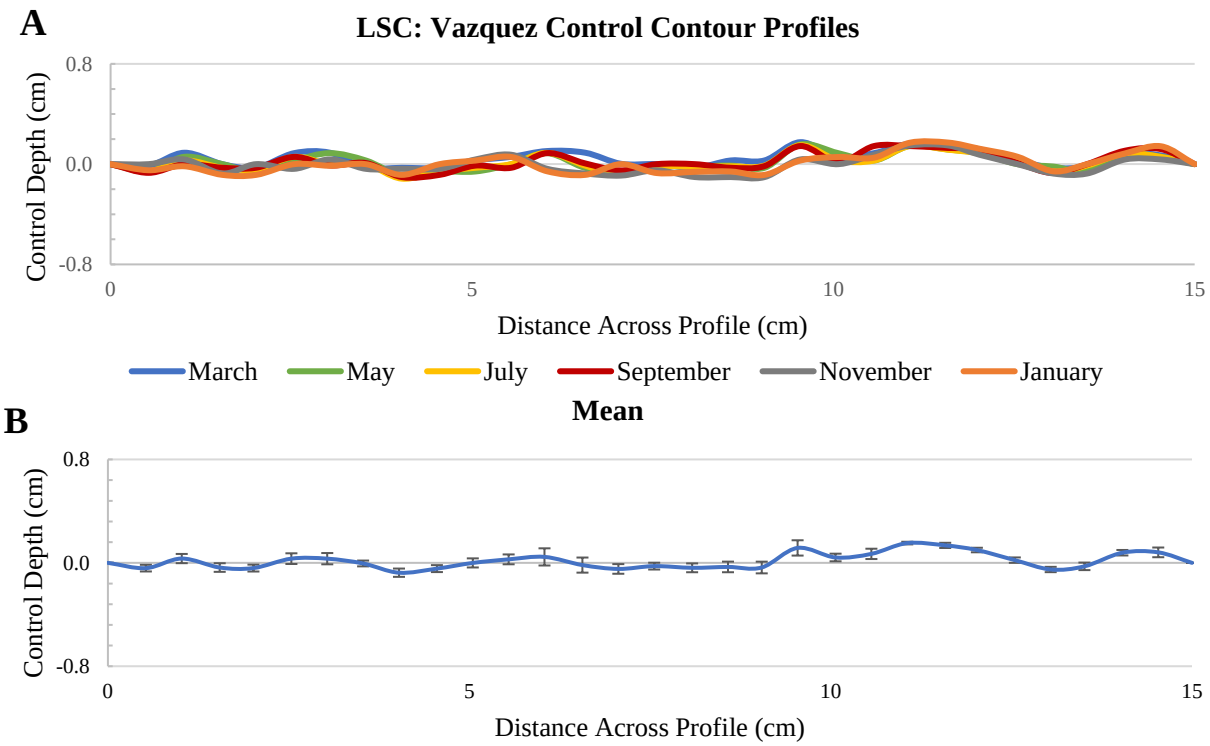

A2: LaSalle Canyon's "*Vazquez"* control and respective mean contour profiles from March 22' to January 23'. **A)** "*Vazquez"* control profiles. **B)** "*Vazquez"* control mean profile.

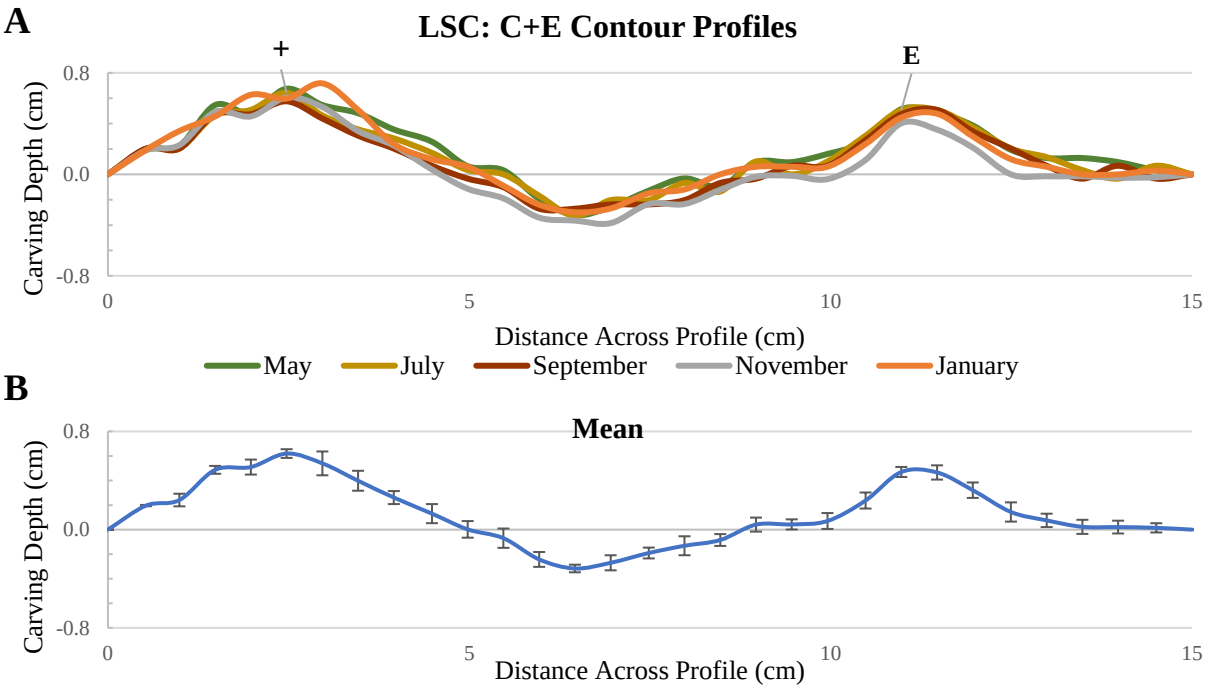

A3: LaSalle Canyon's "*C+E"* carving and respective mean profiles from May 22' to January 23'. **A)** "*C+E"* profiles. **B) "***C+E"* mean profile.

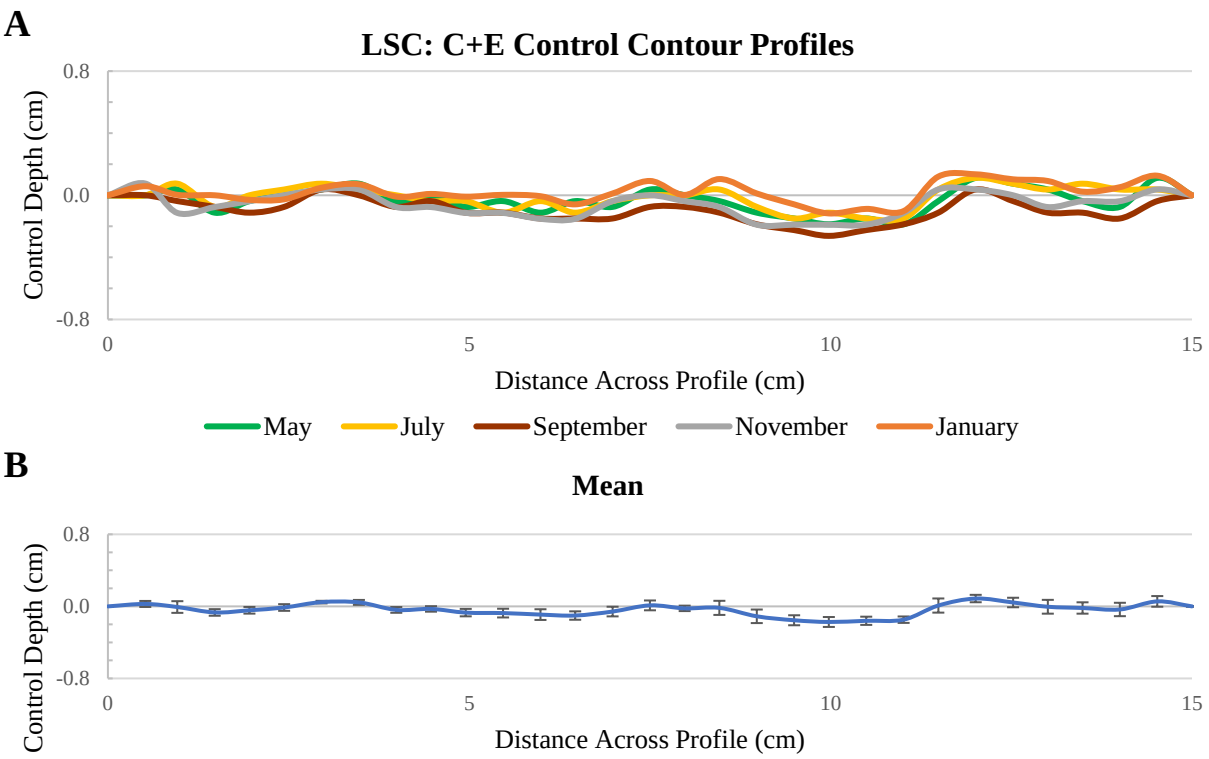

A4: LaSalle Canyon's "*C+E"* control and respective mean profiles from May 22' to January 23'. **A)** "*C+E"* control profiles. **B)** "*C+E"* mean profile.

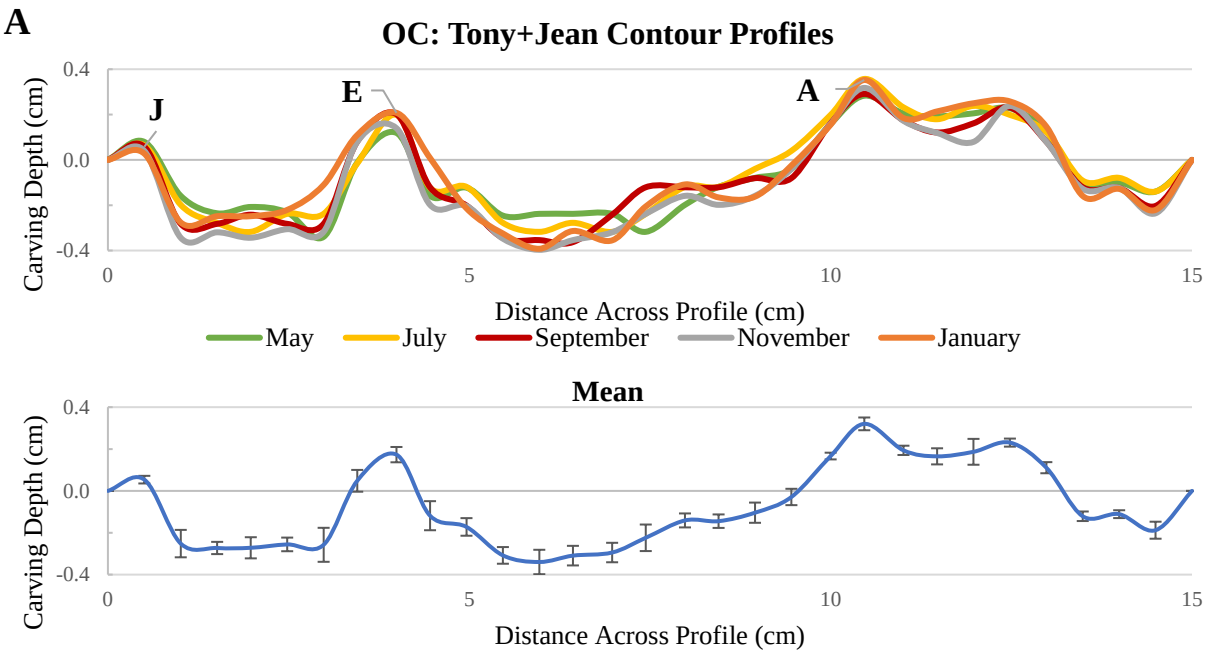

A5: Ottawa Canyon's "*Tony + Jean"* carving and respective mean profiles from May 22' to January 23'. **A)** "*Tony + Jean"* profiles. **B)** "*Tony + Jean"* mean profile.

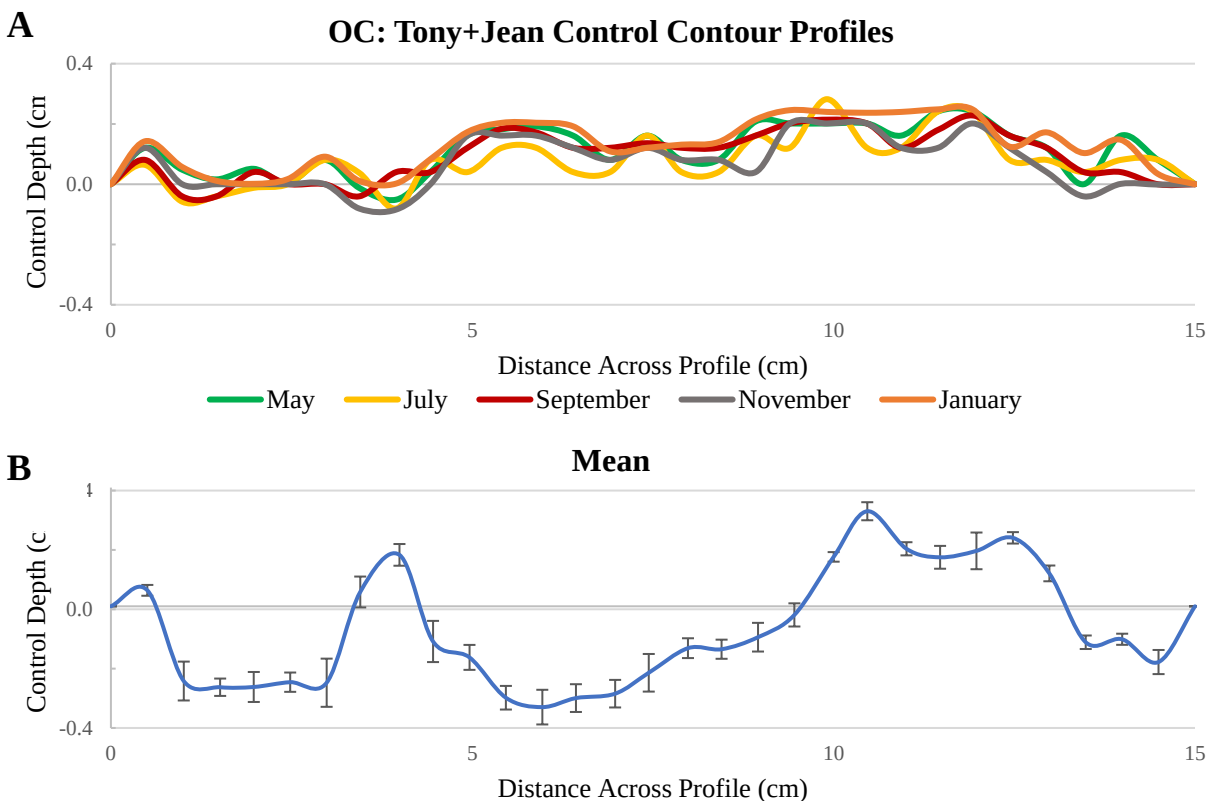

A6: Ottawa Canyon "*Tony + Jean"* control and respective mean profiles from May 22' to January 23'. **A)** "*Tony + Jean"* control profiles. **B) "***Tony + Jean"* mean profile.

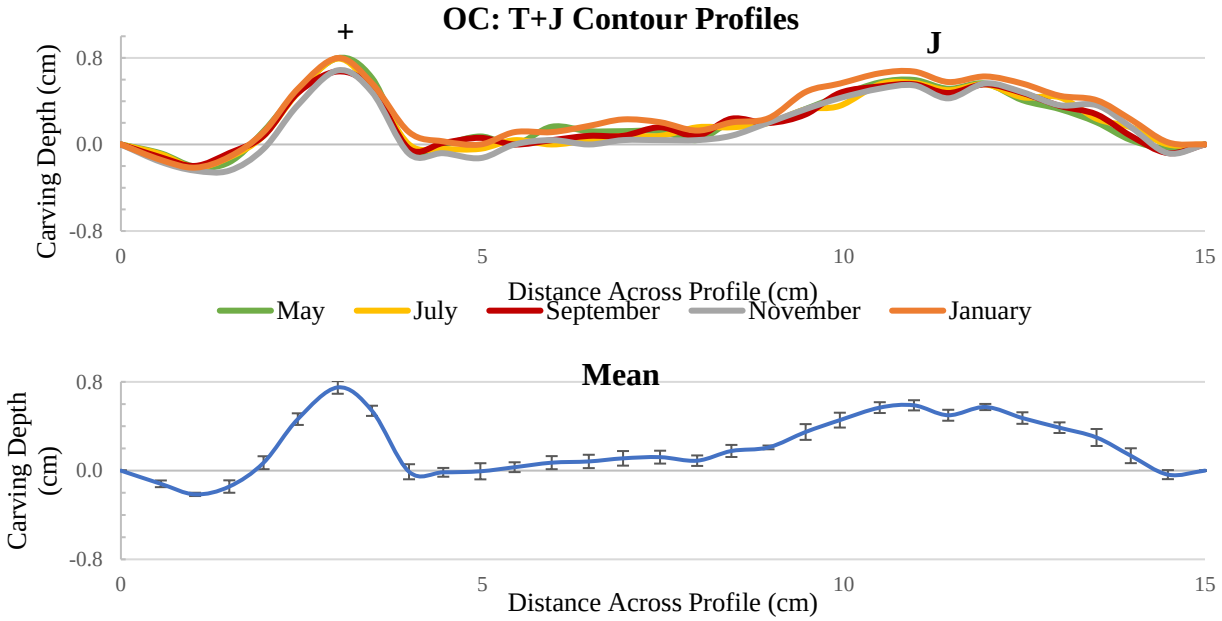

A7: Ottawa Canyon "*T+J"* carving and respective mean profiles from May 22' to January 23'. **A)** "*T+J"* profiles. **B)** "*T+J"* mean profile.

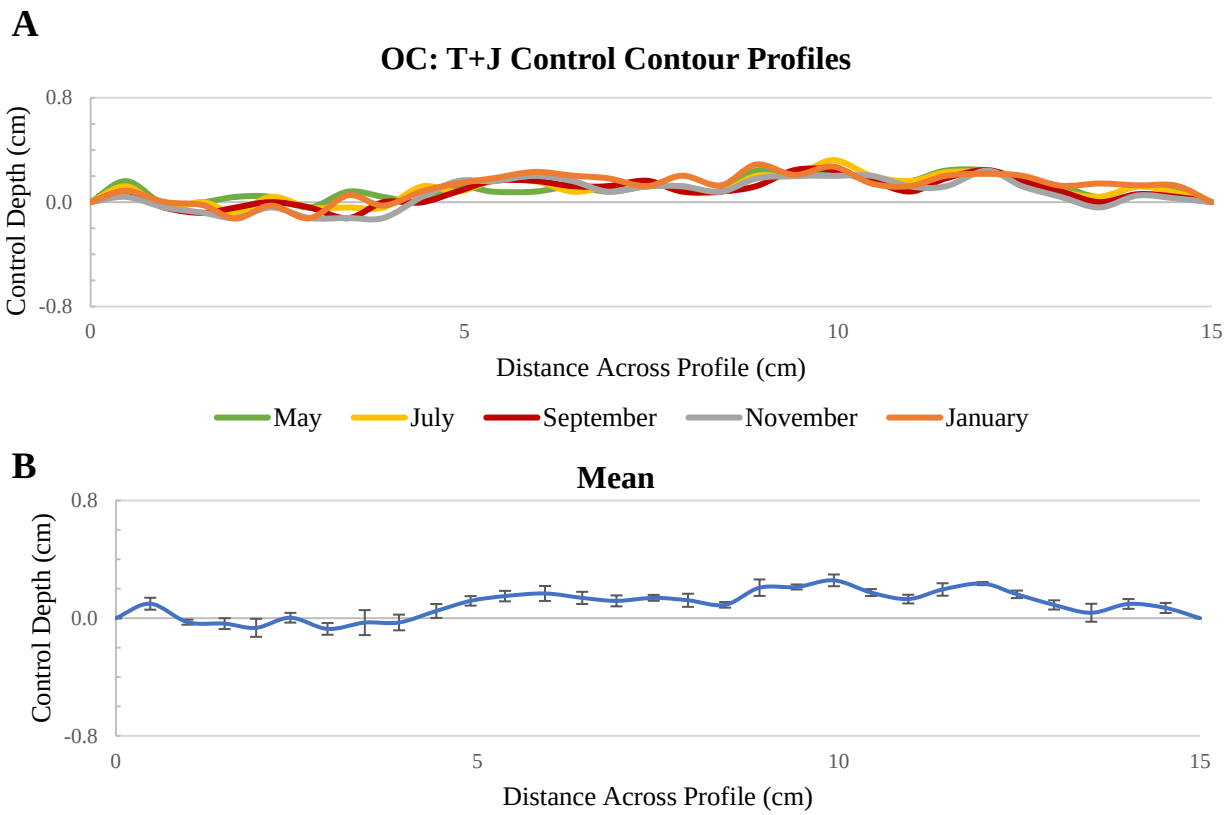

A8: Ottawa Canyon's "*T+J"* control and respective mean profiles from May 22' to January 23'. **A)** "*T+J"* control profiles. **B)** "*T+J"* mean profile.

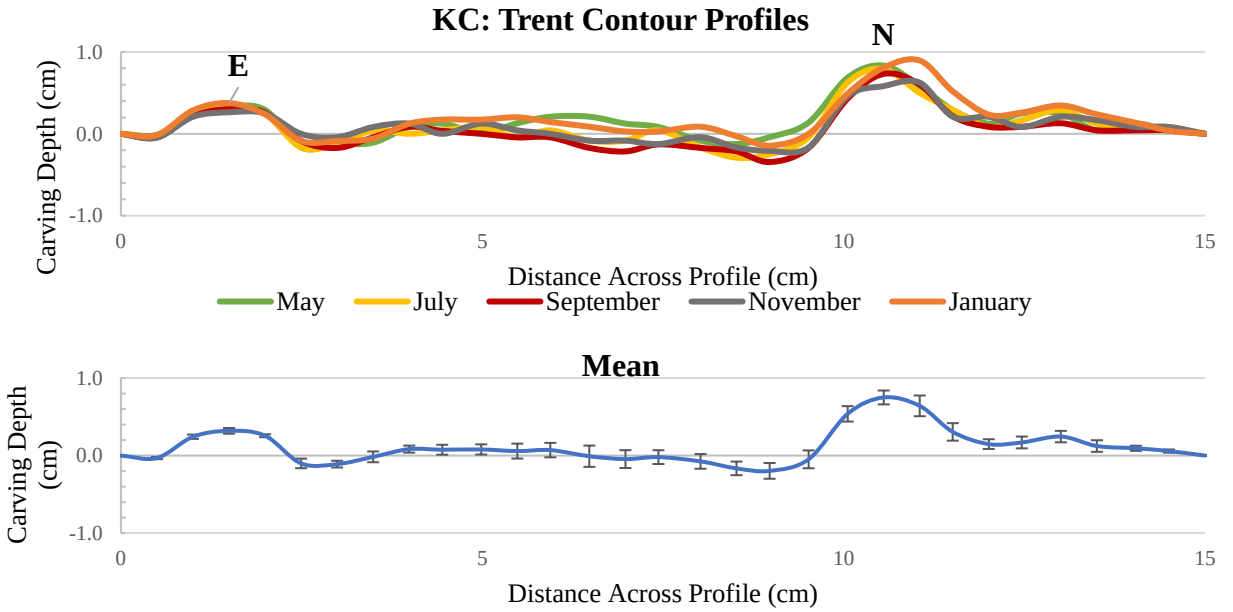

A9: Kaskaskia Canyon's *"Trent"* carving and respective mean profiles from May 22' to January 23'. **A)** "*Trent"* profiles. **B)** "*Trent"* mean profile.

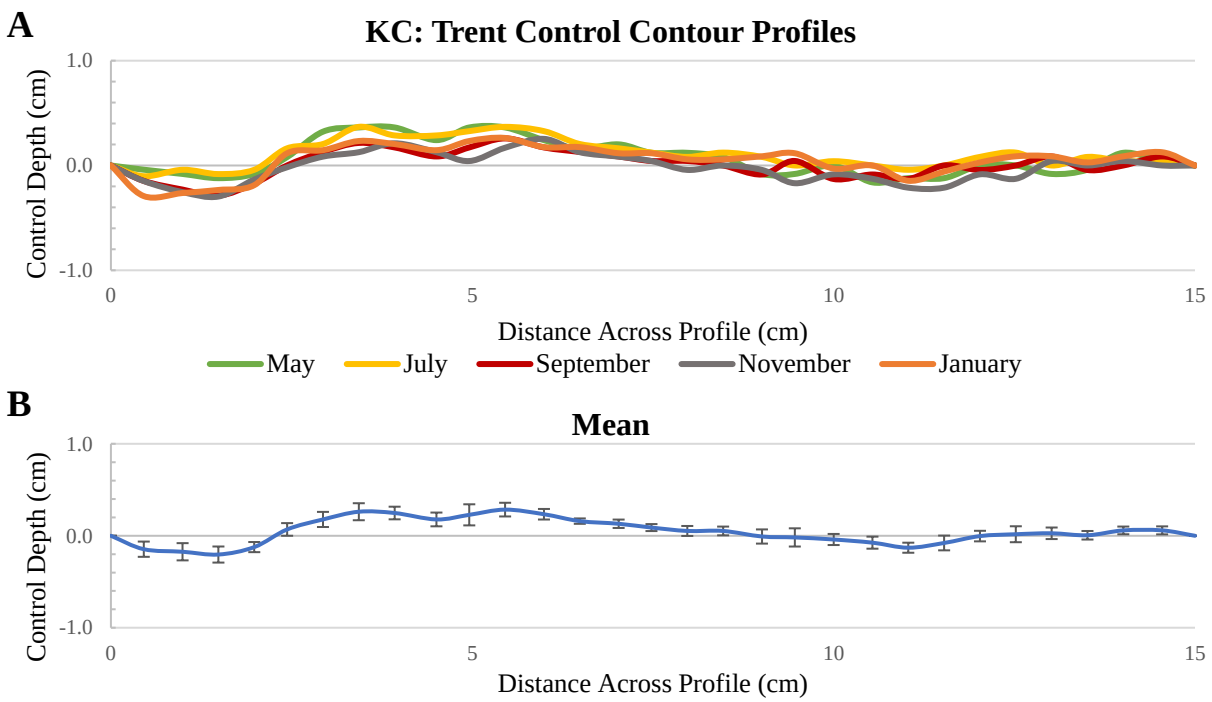

A10: Kaskaskia Canyon's "*Trent"* control and respective mean profiles from May 22' to January 23'. **A)** "*Trent"* control profiles. **B)** "*Trent"* mean profile.

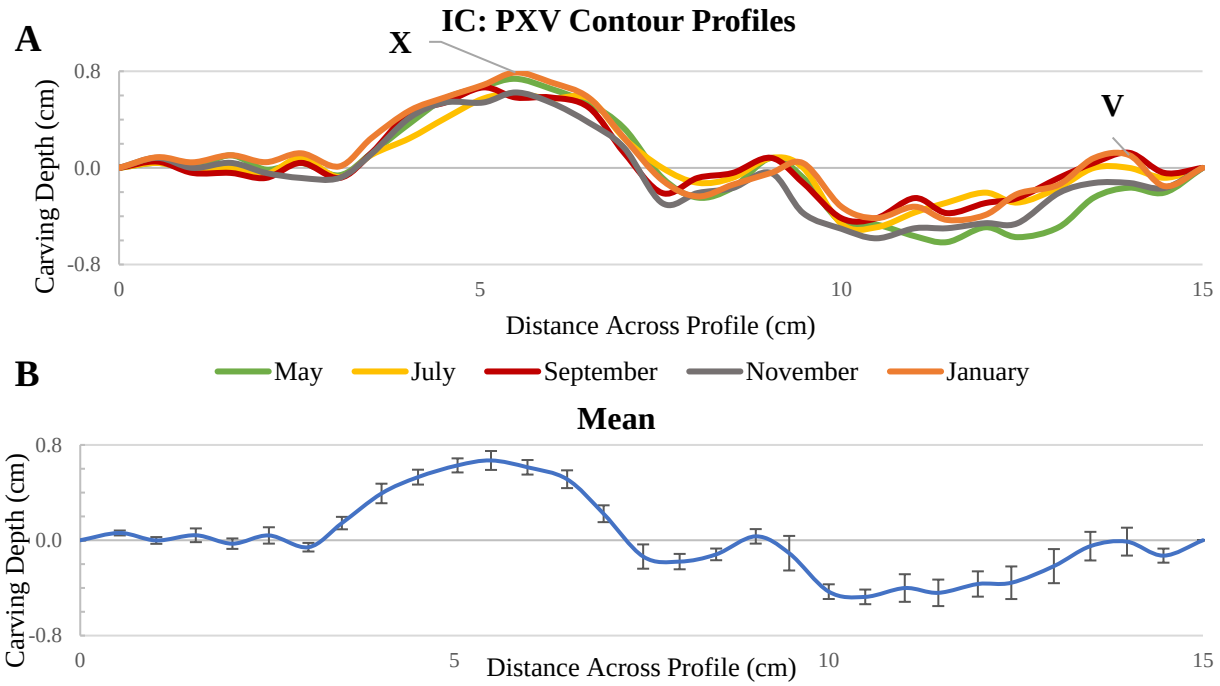

A11: Illinois Canyon's "*PXV"* carving and respective mean profiles from May 22' to January 23'. **A)** **"***PXV"* profiles. **B)** "*PXV"* mean profile.

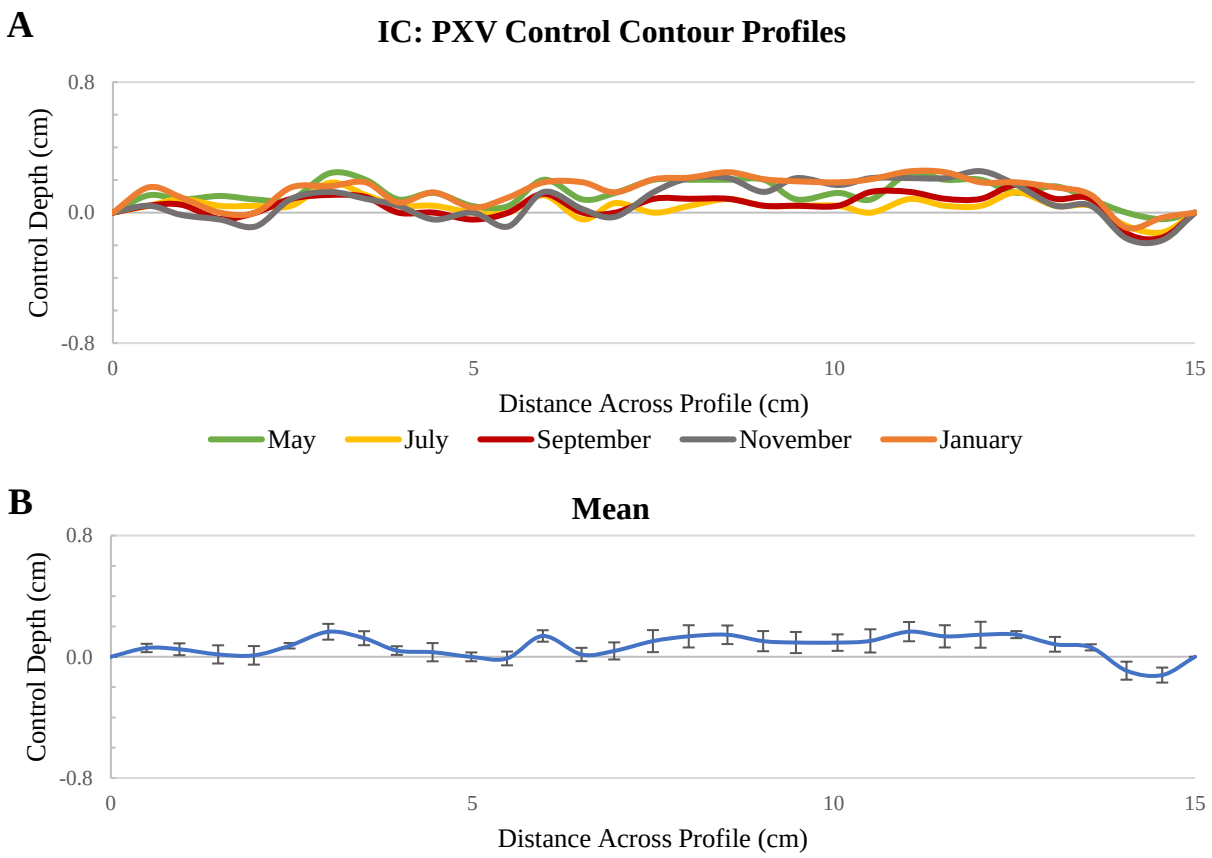

A12: Illinois Canyon's *"PXV"* control and respective mean profiles from May 22' to January 23'. **A)** *"PXV"* control profiles. **B)** *"PXV"* mean profile.